2022

The Role of Pro-Longevity MicroRNAs in Aging

Sarah Noureddine
University of Central Florida

THE ROLE OF PRO-LONGEVITY MICRORNAS IN AGING

by

SARAH ALI NOUREDDINE
B.S. University of Central Florida, 2019
M.S. University of Central Florida, 2021

A dissertation in partial fulfillment of the requirements
for the degree of Doctor of Philosophy
in the Burnett School of Biomedical Sciences
in the College of Medicine
at the University of Central Florida
Orlando, Florida

Fall Term
2022

Major Professor: Michal M. Masternak

ABSTRACT

Cellular senescence, a hallmark of aging, has been implicated in the pathogenesis of many major age-related disorders, including atherosclerosis, metabolic disease, and neurodegenerative disorders such as Alzheimer's disease (AD). AD is characterized by increased cognitive impairment and treatment options available provide minimal disease attenuation. Additionally, diagnostic methods for AD are not conclusive with definitive diagnoses requiring postmortem brain evaluations. Therefore, miRNAs, a class of small, non-coding RNAs, have garnered attention for their ability to regulate a variety of mRNAs and their potential to serve as both therapeutic targets and biomarkers of disease. Several miRNAs have already been implicated with AD and cellular senescence and have been found to directly target genes associated with their pathology. The APP/PS1 mice is an AD model that expresses the human mutated form of the amyloid precursor protein (APP) and presenilin-1 (PS1) genes. In a previous study, crossing long-living growth hormone (GH)-deficient Ames dwarf (df/df) mice with APP/PS1 mice provided protection from AD through a reduction in IGF-1, amyloid-β (Aβ) deposition, and gliosis. Hence, we hypothesized that changes in the expression of miRNAs associated with AD mediated such benefits. To test this hypothesis, we sequenced miRNAs in hippocampi of df/df, wild type (+/+), df/+/APP/PS1 (phenotypically normal APP/PS1), and df/df/APP/PS1 mice. Results of this study demonstrated significantly upregulated and downregulated miRNAs between df/df/APP/PS1 and df/+/APP/PS1 mice that suggest the df/df mutation provides protection from AD progression. Furthermore, we identified a pro-longevity miRNA, miR-449a-5p, downregulated with age in normal mice but maintained in long-living df/df mice. Gene target analysis and our functional study with miR-449a has revealed its potential as an anti-senescence therapeutic. We tested the

hypothesis that miR-449a reduces cellular senescence by targeting senescence-associated genes induced in response to strong mitogenic signals and other damaging stimuli and found miR-449a upregulation reduces senescence, primarily through targeted reduction of $p16^{Ink4a}$, $p21^{Cip1}$, and the PI3K-mTOR signaling pathway. Our results demonstrate that miR-449a is important in modulating key signaling pathways that control cellular senescence and age-related pathologies and that miRNAs hold great potential as therapeutics and/or biomarkers for disease, namely in Alzheimer's disease.

To my parents *Muna* and *Ali Noureddine*,
my loving husband *Mohamad Husseiny*, my siblings, and loved ones –
Thank you for your endless support and words of encouragement,
I dedicate this dissertation to you and to
my beloved uncle *M. Ali* and Grandfather *AbdulRoda Noureddine,*
may their souls rest in peace.

ACKNOWLEDGMENTS

I would like to express my sincere gratitude to my mentor and faculty advisor Dr. Michal M. Masternak. Without his patience, expertise, and guidance this dissertation would not have been possible. His insight and encouragement provided me with the tools necessary to pursue my PhD.

I would also like to thank my dissertation committee members, Drs. Deborah Altomare, Alicja Copik, and Shadab Siddiqi for their constructive and valuable feedback that has helped shape this research and dissertation as well as my experience in the College of Medicine.

My gratitude extends to Drs. Laurence von Kalm and Otto Phanstiel, IV for their kindness and influence in my undergraduate years. Without their reassurance, I would not have pursued this degree.

I am also immeasurably grateful for my previous and current lab-mates and friends, Dr. Allancer Nunes, Sarah Ashiqueali, and Sydney Strader for their collaboration, valued support, and friendship. I am also thankful to Dr. Augusto Schneider for his support and assistance as well as our collaborators at University of Texas (UT) Health Science Center at San Antonio, University of North Dakota, and the Institute for Biogenesis Research at the University of Hawai'i.

I would like to thank Dr. Saleh Naser, Dr. Griffith Parks, Lisa Vaughn, and others at BSBS for their undeniable help and support throughout my graduate studies. I am also greatly appreciative of the recognition and awards they have granted me throughout my years in the program.

Additionally, I would like to express my thanks to the Learning Institute for Elders at UCF (LIFE at UCF) for awarding me the Richard Tucker Gerontology Applied Research Grant that significantly aided me in completing the work presented in this dissertation. I am also greatly

appreciative of the National Institute of Health (NIH) and the National Institute on Aging (NIA) for their financial support as well.

I am furthermore eternally appreciative of all of my family and friends for their endless emotional support.

I would like to especially acknowledge my devoted husband Mohamad Husseiny for his patience and encouragement. Pursuing my academic and professional goals would not have been achieved without his constant, unwavering support.

My sincerest gratitude goes to my parents Dr. Ali and Muna Noureddine; it would not have been possible for me to get this far without their and my siblings' faith in me.

Thank you for everything that you have *all* done for me.

TABLE OF CONTENTS

LIST OF FIGURES

LIST OF TABLES

LIST OF ABBREVIATIONS

AD	Alzheimer's disease
ADAM10	ADAM Metallopeptidase Domain 10
ADSC	Adipose-derived stem cell
AKT	Ak strain transforming
AMPK	5' adenosine monophosphate-activated protein kinase
APBA1	Amyloid Beta Precursor Protein Binding Family A Member 1
APC	Adipocyte precursor cell
APP	Amyloid precursor protein
ATM	Ataxia-telangiectasia mutated
ATR	ATM-and Rad3-related
Aβ	Amyloid-β
BACE-1	β-site amyloid precursor protein cleaving enzyme 1
BCL2	B-cell lymphoma 2
BDNF	Brain-derived neurotrophic factor
CDK	Cyclin dependent kinase
cDNA	Complimentary DNA
CPA	Committed preadipocyte

Df	Dwarf
DNA	Deoxyribose nucleic acid
ErbB/EGFR	Epidermal growth factor receptor
EV	Extracellular vesicle
eWAT	Epididymal white adipose tissue
FACS	Fluorescence activated cell sorting
FAP	Fibroadipogenic precursor
FDR	False discovery rates
FIP	Fibro-inflammatory cell
GH	Growth hormone
GHRH	Growth hormone releasing hormone
HUVECs	Human umbilical vein endothelial cells
IGF-1	Insulin-like growth factor 1
IL	Interleukin
IRS	Insulin receptor substrate
JAK	Janus activating kinase
logCPM	Logarithmic counts per million
logFC	Logarithmic fold change

MAPK	Mitogen-activating protein kinase
MCP	Monocyte chemoattractant protein
MIP	Macrophage inflammatory protein
miRdb	miRNA database
miRNA/miR	microRNA
mRNA	messenger RNA
MSCs	Mesenchymal stem cells
mtDNA	Mitochondrial DNA
mTOR	Mammalian target of rapamycin
$p16^{INK4a}$	p16/cyclin-dependent kinase inhibitor 2A
$p21^{Cip1}$	p21/cyclin-dependent kinase inhibitor 1
PCR	Polymerase chain reaction
PDGFR	Platelet-derived growth factor receptor
Pi3K	Phosphatidylinositol-3-kinase
pRb	Phosphorylated retinoblastoma protein
Prop1	Prophet of Pit1
PS1	Presinilin-1
Rb	Retinoblastoma protein

RNA	Ribose nucleic acid
ROS	Reactive oxygen species
RT-qPCR	Real-time quantitative PCR
SA	Senescence-associated
SAMP8	Senescence accelerated mouse prone 8
SAMR1	Senescence accelerated mouse resistance 1
SASP	Senescence-associated secretory phenotype
SA-βgal	Senescence-associated β-galactosidase
SEM	Standard error of the mean
SnCs	Senescent cells
snRNA-seq	Single nuclei sequencing
STAT	Signal transducer and activator of transcription
TGF- β	Transforming growth factor - β
TSH	Thyroid-stimulating hormone
UMAP	Uniform manifold approximation and projection for dimension reduction
VEGF	Vascular endothelial growth factor
VFR	Visceral fat removal
vWAT	Visceral white adipose tissue

CHAPTER ONE: INTRODUCTION TO AGING, CELLULAR SENESCENCE, AND MICRORNAS

Aging and the Hallmarks of Aging

While aging is a naturally occurring feature in living organisms, the steady loss of function that accumulates at a molecular, cellular, and tissue level with time can give rise to fatal ailments such as organ failure, neurodegenerative disorders, insulin sensitivity, and many others including bone and muscle related diseases [1]. In addition to degenerative diseases, hyperplasia can also occur with time, ultimately resulting in the progression of various types of cancers [1, 2]. The molecular and cellular changes that occur with age have been categorized as major contributors to the aging phenotype and are collectively known as the hallmarks of aging [3]. These hallmarks of aging include genomic instability, telomere attrition, epigenetic alterations, loss of proteostasis, deregulated nutrient sensing, mitochondrial dysfunction, stem cell exhaustion, altered intracellular communication, and cellular senescence [3].

Genomic Instability and Telomere Attrition

Over the course of an organism's life, DNA within cells is replicated as these cells continue to proliferate and divide. Through the process of cellular proliferation, errors in DNA replication can accumulate and contribute to loss of integrity within the genome [4]. Damages including mutations, telomere shortening, integration of viruses, chromosomal loss, translocations, and chromosomal gains that occur naturally with age can collectively and individually contribute to genomic instability and accelerated aging [3]. These changes are not only limited to nuclear DNA, but can also affect mitochondrial DNA (mtDNA), exacerbating mitochondrial dysfunction thereby contributing to aging and the progression of age-associated diseases. Furthermore, genomic instability is implicated in the attrition of telomeres, chromosomal ends that define the proliferative

capacity of a cell [3, 5]. With age, telomere attrition is described as the progressive shortening in length of the ends of chromosomes – a phenomenon that can contribute to increased cell death and cell cycle arrest, thereby advancing the aging phenotype [3].

Epigenetic Alterations

In addition to accumulating damages to DNA and telomeres, specific mechanisms that regulate gene expression are implicated in creating permanent changes to the genome. These changes – independent of genetically inherited patterns of expression – occur with time and are referred to as epigenetic alterations. Epigenetic changes involve DNA methylation, post-translational modification of histones, and chromatin remodeling [3]. DNA methylation is an epigenetic process involving the transfer of a methyl group to a carbon residue on DNA, effectively inhibiting transcription factors from binding to the methylated region and resulting in overall repressed expression of coding and non-coding genes within [6]. Histone modifications, on the other hand, alter the extent to which DNA is wrapped around each histone (protein complex found in chromatin), leading to changes in gene expression patterns as a result of accessibility (or inaccessibility) of the DNA region that is either tightly wound (heterochromatin) or loosely wound (euchromatin) [7]. In addition to DNA methylation and histone modifications, changes in chromatin from an inactive state to a transcriptionally active state can alter the architecture of chromosomes and contribute to epigenetic changes that affect essential age-related pathways including, intracellular processes, inflammation, and nutrient sensing pathways [3].

Deregulated Nutrient Sensing

Availability of nutrients within the tissue microenvironment is essential for the replicative and functional capacities of cells. Reduced nutrient-related signaling and nutrient-reserve availability can negatively influence the viability of a cell and can lead to accelerated cellular aging

[3, 8]. Nutrient reserves are typically stored in the form of glycogen in the liver, muscle and visceral adipose tissue, which play essential roles in providing sources of energy and in regulating various cellular processes related to metabolism [8]. With age, metabolism is significantly affected by specific pathways involved in nutrient sensing that employ four key protein groups – insulin-like growth factor-1 (IGF-1), mammalian target of rapamycin (mTOR), sirtuins, and 5' adenosine monophosphate-activated protein kinase (AMPK) [8]. While maintained expression of sirtuins and AMPK is associated with enhanced longevity, upregulation of IGF-1 and mTOR are typically associated with the opposite phenotype. Several animal models of reduced IGF-1/Growth hormone (GH) have demonstrated significant lifespan extension specifically associated with reduced Pi3K-AKT-mTOR expression [9]. As is evident in figure 1, GH – which promotes expression of IGF-1 – activates the Pi3K-AKT signaling cascade that subsequently activates mTOR. Although both IGF-1 and mTOR are necessary for growth and anabolic metabolism, increased mTOR activity has been found to negatively influence aging and promote cellular senescence [10].

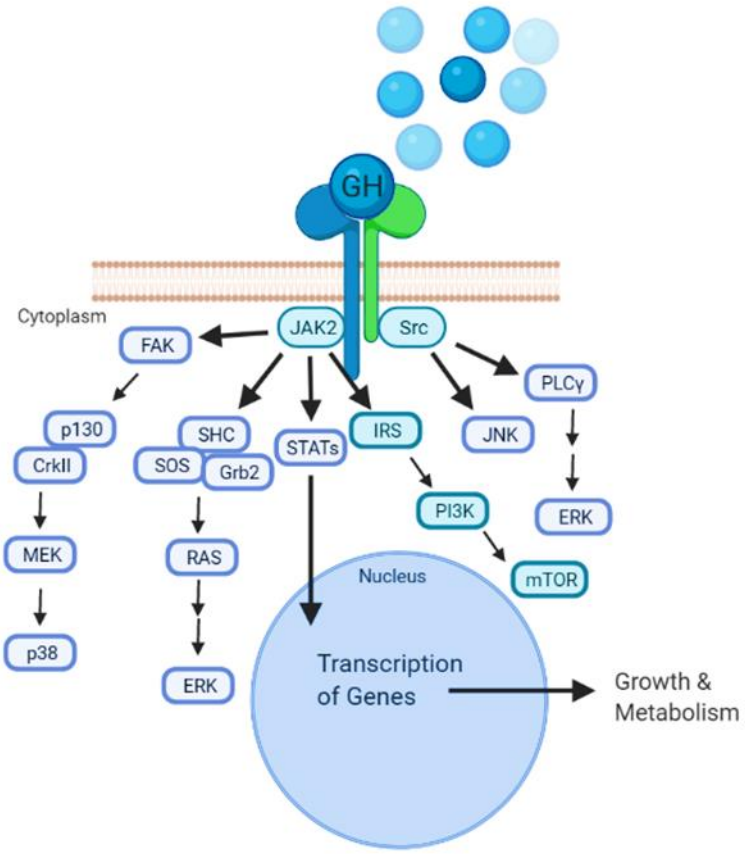

Figure 1: Activation of signaling pathways induced by GH.

(Figure made with BioRender)

Cellular Senescence

It is widely accepted in the fields of cancer and aging research that one common biological phenomenon, and hallmark of aging, contributes to the debilitating progression of diseases with age: cellular senescence. Senescence is a cellular stress response that ultimately results in chronically inactive cells incapable of replicating. The senescence pathway is triggered by a number of varying stressors including DNA damage, telomere shortening, oxidative stress, chromatin disruption, oncogenic activation, and even exposure to mitogenic signals such as growth

hormone (GH) that ultimately result in damage to DNA, proteins, and lipids [11]. Senescence can also be experimentally induced through introduction of these stressors in the form of radiation to induce DNA damage, high glucose/diet-induced obesity, mitogenic exposure (e.g. GH), and through aging. In the presence of these stressors, increased reactive oxygen species (ROS) production or activation of the DNA damage response can thereby stimulate one of two signaling pathways that ultimately result in p16 and/or p21 activation (markers of senescence), yielding a senescent cell [2, 12] (*for process, see* Figure 2).

Typically, in the case of DNA damage, p53 is activated through DNA damage sensors ataxia-telangiectasia mutated (ATM) and ATM-and Rad3-related (ATR) [13]. ATM is activated by double-stranded DNA breaks. In contrast, ATR can respond to a variety of damages to DNA such as lesions that interfere with replication [13]. As DNA damage effectors, ATM and ATR can then activate downstream kinases that ultimately contribute to DNA repair, cell-cycle arrest, or apoptosis [13]. During DNA repair, a replication fork will form to aid in the repair process, however, if the damage is not fixed then the cell receives signals to enter cell cycle arrest [13]. This is carried out by increased expression of p21. Both p16 and p21 are cyclin-dependent kinase (CDK) inhibitors that function by preventing G_1 cyclin-CDK complexes from phosphorylating the retinoblastoma protein (Rb) (Figure 2) [14]. In doing so, the transcription factor E2F remains in complex with Rb and is unable to promote the transcription of growth-related genes necessary for progression into the next phase of the cell cycle. This effectively results in cell cycle arrest [15]. Under non-senescent conditions, with p16 and p21 expressed at low levels, cyclin-CDK complexes phosphorylate Rb, effectively inhibiting pRb from binding to the transactivation domain of E2F. As such, E2F can carry out its function as a transcription factor by promoting the expression of other cyclins such as Cdc25 and Cyclin A [15].

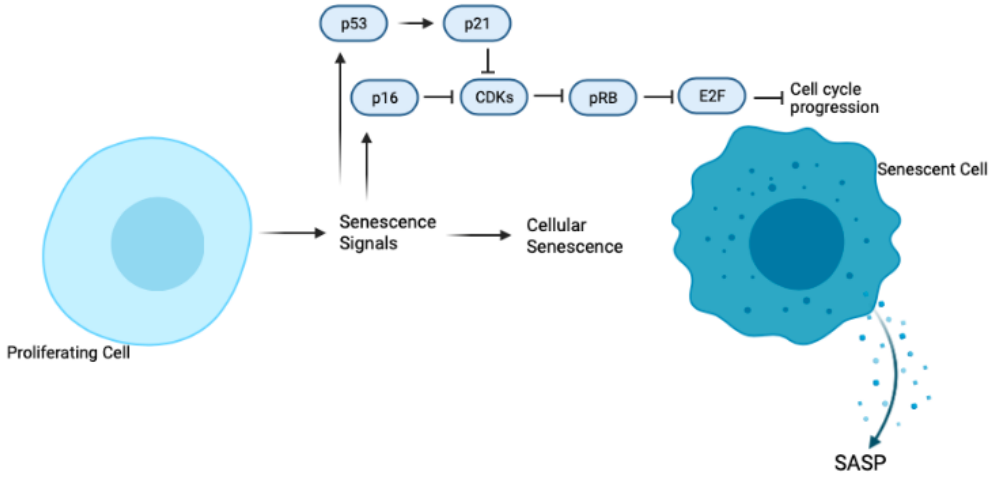

Figure 2: Schematic representation of the senescent pathway.

(Figure made with BioRender)

Cellular senescence has functional benefits in targeting and reducing the proliferative nature of cancer and tumor cells, however, the accumulation of senescent cells can contribute to the opposite: hyperplasia (the abnormal replication of cells) and tissue dysfunction. This is further exemplified by researcher Dr. Judith Campsi, wherein her research has found profound evidence linking the role of senescence in driving hyperplasia, tissue dysfunction, and age-associated disease outcomes to the associated senescence phenotype. Said phenotype is a secretory production that is primarily associated with chronic inflammation [1]. This secretory phenotype, or rather the SASP (senescence-associated secretory phenotype), comprises inflammatory cytokines and chemokines as well as proteases and growth factors released by senescent cells into the extracellular matrix [16]. Some well-known SASP factors include monocyte chemoattractant

protein (MCP) 2 and 4, interleukins 6, 7, 1a, 1b, 13, and 15, macrophage inflammatory proteins (MIP) 1a and 3a, as well as chemokines CXCL and CCL [16]. These factors can stimulate a variety of cellular mechanisms in neighboring cells. Stimulation includes, but is not limited to, inflammation, cell survival, angiogenesis, and even reinforcement of the senescent phenotype. Hence, accumulating senescent cells can alter the tissue microenvironment. This is primarily achieved through the SASP, thereby contributing to altered regulation of a variety of key signaling pathway proteins as well as regulatory microRNAs (miRNAs) [11, 16].

However, despite the apparent transient benefits of the SASP, the secretion of these factors has also been linked to the progression of age-related pathologies due to the growing evidence supporting the role of the SASP in contributing to chronic inflammation, an important contributor in most diseases with age [1, 12]. Furthermore, senescent-associated (SA) pathways are capable of altering expression of transcription factors involved in regulating miRNA transcription and maturation, which can thereby significantly alter the metabolism and homeostasis of a cell and its surrounding microenvironment [11]. Presently, senotherapeutics commonly subcategorized into senolytics and senomorphics have shown great promise in targeting senescent cells and reducing the affiliated SASP. Senolytics are a class of drugs used to clear senescent cells. The most studied senolytics include clude navitoclax, nicotinamide riboside, Fisetin, curcumin, and danazol [17]. However, concerns regarding their toxicity associated with long-term usage, namely with senolytics Dasatinib and Quercetin (D+Q), the former of which is a chemotherapeutic, have been cited [17, 18]. As such, reducing the accumulation of senescence using novel therapies is crucial to diminishing the progression of age-related degenerative diseases and cancers without the associated side effects and toxicity of current methods. Moreover, targeting senescence and its

affiliated secretory phenotype could contribute to enhanced longevity, a notion that is validated in the long-living GH-deficient Ames Dwarf mouse model [19].

Growth Hormone-Deficiency in the Ames Dwarf Mouse

Life-extended Ames Dwarf (df/df) mice are characterized by their loss of function mutation in the Prophet of Pit1 (prop1) gene, necessary for the development of the pituitary gland and its respective function. These df/df mice are thus deficient in GH, prolactin, and thyroid-stimulating hormone (TSH) leading to overall developmental and phenotypic differences between them and their normal littermates [20]. Despite being smaller in structure and pre-disposed to hypothyroidism, df/df mice experience 40-60% increased lifespans with overall improved health [21, 22]. These mice are resistant to cellular and mitochondrial oxidative stress, experience reduced inflammation and senescent burden, and exhibit increased protection from metabolic dysfunction, diabetes, and other age-related diseases such as cancers [22, 23].

Many researchers attribute this improved healthspan and enhanced longevity mainly to the absence of GH, namely due to the observed reduced longevity in df/df mice following GH exposure as early as two weeks of age. This exposure to GH was reportedly followed by reduced cellular stress resistance and increased inflammation, thereby solidifying the pro-aging role of GH [24, 25]. GH is a hormone that is primarily secreted by the pituitary gland in response to the growth-hormone releasing hormone (GHRH) secreted by the hypothalamus. GHRH is secreted in response to the body's need for GH, which includes stimuli in the form of sleep, exercise, nutrition, hunger, and stress [26]. Upon its release, GH travels through the bloodstream and interacts directly and indirectly with the liver, muscle, skeletal tissue, and adipose tissue. The direct mechanism of action involves the binding of GH to effector cells to trigger a response while the indirect

mechanism of action encompasses the effector IGF-1, which is upregulated in response to GH binding to its compatible receptor. Once bound, GH triggers the activation of the Janus activating tyrosine kinases (JAKs) that bind and activate STATs transcription factors necessary for the production of IGF-1 [26]. However, in addition to the activation of the JAK-STATs pathway, other signaling cascades are correspondingly activated in response, including the GH antagonist somatostatin [26].

Of particular interest to this study, the Pi3K-AKT-mTOR pathway is similarly upregulated in the presence of GH (Figure 1). As discussed previously, increased mTOR activity is widely associated with reduced longevity, a phenotype observed in df/df mice as well [9, 10]. These long-living mice not only experience low levels of IGF-1 due to their GH-deficiency but also exhibit reduced mTOR activity in tissue responsive to IGF-1, such as visceral adipose tissue, and enhanced insulin sensitivity overall [9, 19]. Prior studies from our lab have moreover demonstrated a correlation between increased insulin resistance and visceral fat removal (VFR) in long-living df/df mice, while phenotypically normal mice experienced enhanced insulin resistance following VFR [27]. These findings suggest df/df mice experience increased healthspan directly aligned with their altered adipose composition and GH-deficiency. As such, long-living df/df mutant mice and their phenotypically normal littermates serve as the ideal models for studying molecular and genetic changes controlling gene expression that are affected by GH and cellular senescence.

microRNAs

microRNAs (miRNAs) are small, non-coding RNAs typically 20-25 nucleotides in length that regulate gene expression at the post-transcriptional level [28]. These small RNAs have recently garnered attention for their ability to regulate a variety of signaling pathways and cellular

mechanisms by binding to and targeting complimentary messenger RNA (mRNA) transcripts [29]. In doing so, mature miRNAs are capable of repressing translation of their target mRNAs. miRNAs are typically processed by Drosha and Dicer RNase-III enzymes into double-stranded RNA duplexes that contain both the mature and complimentary miRNA strands designated as the 5p fragments and the 3p fragments, respectively [28]. Expression of these small RNAs have diverse patterns that play a key role in regulating the development of an organism throughout its lifespan. Recent studies have found, however, that aging and certain biological processes can affect the expression patterns of miRNAs [30]. Through altered miRNA expression profiles, the pathways these miRNAs regulate are subsequently affected.

Of particular interest to our research, preliminary data from our lab has revealed a potential role of miRNA-449a-5p (miR-449a) in regulating the senescence pathway, with additional findings indicating a potential link between growth hormone (GH) levels and reduced intracellular expression of miR-449a. Preliminary gene-target analysis using the miRNA database (miRdb) generated a list of potential targets of miR-449a that are associated with the senescent pathway comprising *March5, Map2k1/Map2k3, Ppm1b, Bcl6, Snai1*, and *Axl*. When cross-referenced with the senescence database, these genes demonstrated the capacity to induce senescence when over-expressed, suggesting that miR-449a's predicted role in targeting these genes could serve to reduce senescent outcome [31, 32]. Additionally, Khee et al. found an association between increased senescence and decreased expression of two miRNA's – miRNA-20a and miRNA-449a, noting that a younger phenotype is associated with increased expression of the latter [11]. Researchers at the Institute of Neuroscience in Yunnan correlated increased miR-449a expression with reduced progression of brain aging in mice [33]. Furthermore, previously published results from our lab demonstrated a steady decline in the expression of miR-449a in phenotypically normal mice with

age. However, in long-living GH-deficient Ames Dwarf (df/df) mice, this miRNA was steadily expressed throughout their lifespan [30]. The release of GH – which triggers STATs, ERK1/2, AKT, and mTOR signaling pathways – is suspected to promote senescence through the transcription of growth and metabolism-related genes as described previously [12, 34]. Since strong mitogenic signals have formerly been implicated with driving cells into senescence, the research presented here is thus centered on investigating the effects of GH, among other factors, on cellular senescence and age-related pathologies. Moreover, preliminary findings from our lab have shown increased expression of miR-449a in adipose-derived mesenchymal stem cells (ADSCs), leading us to speculate that this miRNA may contribute to the regenerative effects of these stem cells. As such, there is compelling evidence supporting the therapeutic potential of miR-449a in reducing the progression of age-related pathologies primarily through regulating senescent pathways. The findings outlined in this study aim to provide added insight into the effects of age and genotype on the expression of miRNAs such as miR-449a and the pathways they regulate as well as the important role miRNAs play in disease progression such as Alzheimer's disease (AD).

In addition to the apparent role of miRNAs in regulating intracellular pathways, and the ostensible effect of cellular senescence on the microenvironment and tissue as a whole, there is a current gap in the field regarding non-toxic anti-senescence therapies. As such, identifying a novel method of reducing cellular senescence without severe adverse effects may solve this current demand in the field. Shifting towards the benefits of non-invasive, easy, and rapid uptake of lipid-tagged miRNAs will likely overcome the invasiveness, toxicity, and potential vaso-occlusive or teratoma formations associated with whole cell therapies. Hence, the findings presented here in chapters two and three further expand on the potential of miRNAs to serve as therapeutics and/or biomarkers of disease.

Alzheimer's Disease

According to the World Health Organization, age-related diseases such as cardiac and pulmonary diseases, cancers, and neurodegenerative diseases, account for approximately twenty million deaths annually worldwide [35]. Currently, Alzheimer's disease (AD) is the seventh leading cause of death globally, affecting approximately 6.5 million Americans [36]. As the most prevalent type of dementia, AD is characterized by cognitive impairment, changes in behavior, and inability to perform daily, routine tasks among others [37]. The symptoms of AD are widely attributed to the formation of hyperphosphorylated tau neurofibrillary tangles in the brain and amyloid-β (Aβ) plaque accumulation [38]. Aβ is produced through irreversible post-translational processing of the amyloid precursor protein (APP) carried out by β- and γ- secretases, enzymes that cleave APP to yield Aβ. According to the amyloid hypothesis, Aβ is suggested to be the main cause of AD through accumulation of the peptide into plaques that commonly develop and aggregate in the hippocampus, neocortex, and cerebrovasculature [39]. Although Aβ toxicity is predicted to be the primary contributor to AD pathology, neurofibrillary tangles formed by hyperphosphorylated tau contribute significantly to neurofibrillary degeneration and subsequently to neuronal dysfunction [40]. Hence, both abnormal filaments augment neuronal cell degeneration and progressive dementia; however, the exact mechanism remains unknown.

AD has also been linked to increased reactive oxygen species (ROS) production with specific mutations in the APP and presenilin-1 (PS1) genes ultimately contributing to APP processing and Aβ deposition [39]. The accompanying damage observed in human AD brains can also be modeled in APP/PS1 transgenic mice, which express the human mutations for APP and PS1 and have been found to exhibit similar outcomes such as increased Aβ. Aging is primarily the

largest risk factor for AD progression, with plaques and tangles forming sporadically in growing individuals. As a result, researchers at the University of North Dakota School of Medicine and Health Sciences investigated the potential protective benefits of GH-deficient df/df mice in AD progression by crossing dwarf mice with APP/PS1 transgenic mice. The resulting F2 generation consisted of phenotypically normal APP/PS1 mice and df/df/APP/PS1 mice that allowed for analysis of the effect of changes in genotype on AD pathology. This study demonstrated a significant reduction in Aβ levels in df/df/APP/PS1 transgenic mice, suggesting the absence of GH conferred protective advantages against AD. Hence, we were interested in investigating the changes in miRNA expression profiles that could be contributing to the observed protective advantages as well as exploring the potential interrelatedness of AD, deregulated nutrient sensing in the brain, and the GH/IGF-1 axis.

Dissertation Hypothesis

Based on the above-described changes in gene expression patterns that correspond to age and the aging phenotype, as well as the apparent importance of miRNAs in regulating a large subset of pathways required for maintaining normal cellular processes and tissue composition, it is fundamentally crucial to address the gap in understanding of the therapeutic potential of miRNAs in age related diseases and disorders. Currently, there are clinical explorations of therapies to derive efficacy in reducing or targeting cellular senescence, a major contributor to age-related pathologies and one of nine hallmarks of aging. Despite the promise that these therapies (namely, senolytics and senomorphics) hold, there are pressing concerns for the overall toxicity and predicted side effects associated with their administration that require novel solutions with similar therapeutic efficiencies [18].

Furthermore, exploring preventative measures that will allow for delaying the onset of both senescence and the progression of age-related pathologies is crucial for advancing clinically available methods in the field of aging and metabolism in addition to diversifying the means through which these therapies function. Hence, the research presented in this dissertation aims to provide sufficient support for the development of a novel anti-senescent therapeutic utilizing miR-449a that will a) address a current gap in the field regarding non-invasive anti-aging therapies, and b) target cellular senescence.

Through the study presented in chapter 2, we tested the hypothesis that long-living df/df mice encompass healthier adipose tissue composition that serves as a youthful source of miR-449a, a miRNA that reduces cellular senescence by targeting the senescent pathway. In doing so, we classified the cell types within adipose tissue of df/df mice and derived the full mechanistic and functional role of miR-449a and its potential as a therapeutic in reducing the development of age-related pathologies aggravated by cellular senescence through an onset of mitogenic signals (e.g., GH). We also evaluated the potential of miR-449a in enhancing the regenerative effects of human stem cells.

In chapter 3, we explored the greater potential of miRNAs in a disease model comprising APP/PS1 transgenic mice expressing the human mutations for APP and PS1 that contribute to human AD, and explored the premise that miRNAs involved in regulating APP and Aβ levels in the brain of APP/PS1 mice are significantly altered by the df/df phenotype. We identified a group of differentially expressed miRNAs that may serve as therapeutic targets and/or biomarkers of disease, a clinically significant finding that could advance diagnostic methods for AD.
The findings outlined in these chapters provide added insight into the role of GH and miRNAs in aging and age-related pathologies.

CHAPTER TWO: MICRORNA-449A REDUCES GROWTH-HORMONE STIMULATED SENESCENT CELL BURDEN THROUGH PI3K-mTOR SIGNALING

Preface

This chapter is currently under review at the Proceedings of the National Academy of Sciences (PNAS) (Manuscript # 2022-13207).

Noureddine S, Nie J, Scheider A, Fliesen Z, Dhabhi J, Victoria B, Oyer J, Nunes ADC, Ashiqueali S, Copik A, Robbins PD, Musi N, Masternak MM. microRNA-449a reduces growth hormone stimulated senescent cell burden through Pi3k-mTOR signaling. PNAS.

Abstract

Cellular senescence, a hallmark of aging, has been implicated in the pathogenesis of many major age-related disorders, including neurodegeneration, atherosclerosis, and metabolic disease. Therefore, investigating novel methods to reduce or delay the accumulation of senescent cells during aging may attenuate age-related pathologies. microRNA-449a-5p (miR-449a) is a small, non-coding RNA downregulated with age in normal mice but maintained in long-living growth hormone (GH)-deficient Ames Dwarf (df/df) mice. Gene target analysis and our functional study with miR-449a-5p has revealed its potential as a serotherapeutic. Here we test the hypothesis that miR-449a reduces cellular senescence by targeting senescence-associated genes induced in response to strong mitogenic signals and other damaging stimuli. We found increased fibroadipogenic precursor cells, adipose-derived stem cells, andmiR-449a levels in visceral adipose tissue of long-living df/df mice. GH downregulates miR-449a expression and accelerates senescence. miR-449a upregulation using mimetics reduces senescence, primarily through targeted reduction of $p16^{Ink4a}$, $p21^{Cip1}$, and the PI3K-mTOR signaling pathway. Our results demonstrate that miR-449a is important in modulating key signaling pathways that control cellular senescence and the age-related pathologies.

Introduction

Genetic mutant Ames dwarf (df/df) mice, characterized by growth hormone (GH) deficiency, live between 40-60% longer than their normal littermates [21, 22]. These mice also have improved health span, including protection from metabolic syndrome, diabetes, and cancer [22, 23]. However, although these metabolically heathy df/df mice tend to become obese with age, they maintain high insulin sensitivity [27]. While surgical removal of visceral fat improved insulin sensitivity in controls, in obese df/df mice it had the opposite effect [27]. These findings suggest the endocrine system has varied roles in insulin sensitivity in normal mice versus GH-deficient df/df mice. However, the mechanisms responsible for this altered metabolic function of visceral fat on health and longevity are not well understood. Since adipose tissue is composed of heterogeneous cell types [41], its cellular composition likely plays a major role in regulating overall health, including insulin sensitivity, glucose metabolism, and inflammation [42].

Progenitor cells, including pre-adipocytes and adipose-derived stem cells (ADSCs), are important both for tissue health and for overall health. Accumulation of changes that compromise tissue function within these cells can lead to age-related pathologies (e.g. metabolic diseases neurodegenerative, and cardiovascular pathologies) and give rise to various types of cancers [29]. Cellular senescence has a causal role in progression of these age-related pathologies. Senescence, or rather, the state of proliferative arrest, is triggered by multiple stressors, including DNA damage, oncogenic activation, exposure to chronic or unbalanced mitogenic signals such as GH, telomere shortening, and chromatin disruption [1].

Although the senescence response can yield beneficial temporal advantages such as tumor suppression or wound repair, the accumulation of metabolically active senescent cells (SnCs) can contribute to tissue dysfunction, resulting in pathogenic progression [1]. SnCs can alter the tissue

microenvironment primarily through the pro-inflammatory senescence-associated secretory phenotype (SASP), which involves cytokines, chemokines, growth factor metalloproteases, membrane proteins, and extracellular vesicles [16]. SASP factors can stimulate various cellular mechanisms in neighboring cells including, but not limited to, cell proliferation, senescence, and angiogenesis [16]. Despite the apparent transient benefits of the SASP, secretion of the same factors is also linked to progression of age-related pathologies. The SASP contributes to age-dependent chronic inflammation, a key factor in pathogenesis of many age-dependent diseases [29]. Hence, reducing SnC burden can decrease age-dependent pro-inflammatory signals and pathologies. At the same time, maintaining high populations of healthy progenitor cells can counter the negative impact of senescent cells and, in some cases, even suppress senescence in various tissues.

Some drugs or drug combinations can induce apoptosis specifically in senescent cells; however, these senolytic compounds likely have off-target toxicity [42]. As such, identifying a novel method of reducing cellular senescence without severe adverse effects is clinically important. Recently, the role of microRNAs (miRNAs) has been studied due to their ability to target and suppress the translation of messenger RNAs (mRNAs). As a result, miRNAs have been identified as key regulators of many signaling pathways [43, 44] including pathways important for regulating cellular senescence [11]. Furthermore, certain miRNAs are associated with increased lifespan and longevity. Studies from our laboratory with long-living GH-deficient df/df mice identified a variety of miRNAs differentially regulated with age [30]. One of these miRNAs was microRNA-449a-5p (miR-449a). miR-449a expression decreased significantly with aging, yet both long-living GH-deficient mice and older calorie-restricted mice maintained youthful levels of miR-449a in circulation, suggesting its potential role in longevity [30]. Additionally, increased

senescence was associated with decreased expression of miR-20a and miR-449a, and a younger phenotype was associated with increased expression of miR-449a [11]. Thus, there is compelling evidence that miRNA-449a has therapeutic potential for reducing progression of age-related pathologies, primarily through regulating senescence pathways.

Long-living df/df mice also experience reduced senescence onset related to age compared with normal littermates due to GH deficiency [19]. One study demonstrated a direct correlation between GH treatment in df/df mice and increased senescence burden, suggesting GH is involved with inducing accelerated senescence in preadipocytes, including ADSCs [45]. ADSCs typically make up a high proportion of adipose tissue and are essential for tissue repair and regeneration [46]. Despite increased intra-abdominal fat accumulation in df/df mice, our previous study suggests that they have improved metabolic health [27].

Single-cell and single-nuclei sequencing approaches allow in-depth acquisition of genomic and transcriptomic information for identifying differences in cell populations and relationships in a given sample. Such techniques make possible analyses of molecular mechanism as well as smaller cell populations and their heterogeneity allowing characterization of cell populations and production of cell maps. In this study, single-nuclei sequencing (snRNA-seq) was performed in visceral fat from Ames Dwarf mice to compare changes in subpopulations and heterogeneity between df/df mice and phenotypically normal mice. In addition, we evaluated the roles of miR-449a, GH, and adipose-derived stem cells in modulating cellular senescence.

Materials and Methods

Mice and Tissue Collection

Phenotypically normal heterozygous females (N/df) were mated with homozygous Ames dwarf (df/df) males to produce offspring with both normal (N/df) and df/df phenotypes. Mice were bred under controlled temperatures and light cycles and placed on a nutritionally balanced diet (Rodent Laboratory Chow 5001) provided *ad libitum*. For RNA sequencing, male offspring (8-12 months of age) were divided into normal (N/df, n = 4) and dwarf (df/df, n = 5) groups. Mice were anesthetized with 2.5% isoflurane and sacrificed following overnight fasting for tissue collection. Harvested tissue was immediately snap-frozen on dry ice and stored at -80℃.

To perform fluorescence-associated cell sorting (FACS), both male N/df (n = 7) and df/df (n = 7) mice were used. Mice were anesthetized with isoflurane and sacrificed as described previously prior to tissue collection. Skin was disinfected with 70% ethanol prior to adipose depot removal. vWAT obtained from N/df and df/df mice was transferred to 50 mL conical tubes containing 10 mL of ice-cold buffer containing HBSS, 2% FBS, and HEPES (Gibco^{TM}, Waltham, MA). All collected vWAT was weighed to ensure at least 1 g of fat was included and kept on ice for tissue lysis and digestion. Minced tissue (1-2 mm in size) was digested using 0.8 mg/mL Gibco^{TM} collagenase (Type II) diluted in 5 mL of wash buffer and then incubated in a shaking water bath (120-140 rpm) for 60 minutes at 37 °C. Following incubation, samples were centrifuged at 300 x *g* for ten minutes at 4 °C to separate adipocytes (white layer on top) from stromal vascular cells (pre-adipocyte precursors; red/white pellet at the bottom). Separated cells were then prepared for FACS (see section 4.5).

Isolation of Nuclei from Adipose Tissue

The nuclei isolation protocol was adapted from previously published methods [47]. 0.5 to 1 g of subcutaneous WAT was rinsed in ice-cold PBS two times. The tissue was transferred into a Loose Pestle Dounce Tissue Grinder (Electron Microscopy Sciences, Hatfield, PA) containing 1 mL nuclei isolation buffer [10 mM Tris-HCl (Lonza, BE17-737E) (pH 7.4), 3 mM $MgCl_2$ (Sigma-Aldrich, St. Louis, MO), 10 mM NaCl (Sigma-Aldrich), and 0.1% IGEPAL CA-630 (NP-40) (Sigma-Aldrich), in nuclease-free water] on ice. The samples were homogenized by applying 15-20 strokes of the loose pestle. The homogenate was filtered through a 40 μm cell strainer (Fisher Scientific, Portsmouth, NH) and centrifuged at 500 g for 8 min at 4°C. The nuclear pellet was resuspended in 1 mL nuclei isolation buffer containing 0.2 U/μL RNase inhibitor (Invitrogen, Waltham, MA) and centrifuged at 500 g for 8 min at 4°C. Finally, the nuclear pellet was resuspended in 100 μL nuclei resuspension buffer (1% bovine serum albumin in phosphate-buffered saline) and 1 U/μL RNase inhibitor (New England Biolabs, Ipswich, MA). All solutions were sterile-filtered before use. Nuclei were counted in a hemocytometer.

10x Genomics and RNA Sequencing (Single-Cell Sequencing)

The GemCode Single-Cell Instrument (10x Genomics, Pleasanton, CA) and Single Cell 3 Library & Gel Bead Kit v3.1 Kit (10x Genomics) were utilized for single-cell analyses and library preparation. About ~17,400 nuclei were added to each channel with a targeted cell recovery estimate of 10,000 cells. After generating nanoliter-scale Gel bead-in-EMulsions (GEMs), GEMs were reverse-transcribed in a T100 Thermal cycler (Bio-Rad, Hercules, CA) programmed at 53°C for 45 min, 85°C for 5 min, and held at 4°C. All subsequent steps to generate single-cell libraries were performed according to the manufacturer's protocols. Libraries were sequenced with an Illumina NovaSeq 6000 System (North Texas Genome Center, University of Texas at Arlington),

with approximately 80,000 raw reads per nucleus. The libraries were sequenced with the following sequencing parameters: 26 bp read 1 – 8 bp index 1 (i7) – 88 bp read 2.

RNA Sequencing

Visceral fat obtained from N/df (n = 4) and df/df (n = 5) male mice were cut and weighed to obtain approximately 30 mg of tissue for RNA extraction. Samples were homogenized in a bullet blender using 500 µL of QIAzol Lysis Reagent and 0.5 mm zirconium oxide beads for 3 minutes. An additional 400 µL of QIAzol Lysis Reagent was added to each sample following tissue lysis. After complete tissue homogenization was achieved, the manufacturer's protocol was used in accordance with the RNeasy mini kit (QIAGEN; Hilden, Germany). The purified total RNA was then eluted using 30 µL of RNase-free water and nucleic acid quantification was performed using the Epoch Gen5 Plate Reader. One µg of total RNA isolated from each tissue sample was used to construct sequencing libraries with the NEBNext Ultra Directional RNA Library Prep Kit for Illumina (San Diego, CA), following the manufacturer's protocol. Libraries were submitted for 100-bp paired-end sequencing by Illumina HiSEQ 2000 at the Genomics Core in the University of California Riverside (UCR) Institute of Integrated Genome Biology.

Fluorescence-Activated Cell Sorting (FACS)

Previously separated stromal vascular cells comprising pre-adipocyte precursors isolated from adipose depots of N/df (n = 7) and df/df (n = 7) mice were filtered through a 70 µm sterile nylon mesh with 5 mL of wash buffer using a Pasteur pipette. Filtered cells were then centrifuged at 300 x *g* for 5 minutes and incubated at room temperature for 10 minutes with occasional shaking in 1 mL of sterile RBC lysis buffer solution (eBioscience™, San Diego, CA). To neutralize RBC lysis buffer following incubation time, eBioscience™ Flow Cytometry Staining Buffer (FACS buffer) was added. Samples were then centrifuged at 300 x *g* for 5 minutes at 4 °C and subsequently

incubated with eBioscience™ CD16/32 Fc block for 10 minutes at 4 °C. The pellet was then disrupted and incubated for 30 minutes at 4 °C with added FACS buffer and anti-mouse antibody conjugate cocktails containing eBioscience™ anti-Sca-1 (Alexa Fluor700), eBioscience™ anti-lineage cocktail (FITC), BioLegend (San Diego, CA) anti-CD34 (PE), eBioscience™ anti-PDGFRα (anti-CD140a, APC), and eBioscience™ 7-AAD Viability Staining Solution. Cells were then washed twice in FACS buffer and centrifuged at 300 x *g* for 5 minutes. Using Gibco™ StemPro basal media supplemented with 30% fetal bovine serum (FBS), cells were resuspended and immediately analyzed on the cytometer for cell sorting. Cell populations were gated based on the following criteria: Viable (live) cells, lineage (-), PDGFRα (+), Sca-1 (+), or CD34 (+) (Supplementary Figure 3). Cell populations within the aforementioned gates were considered to be adipose-derived stem cells based on a literature survey of known markers [48].

Cell Culture

Human umbilical vein endothelial cells (HUVECs) were cultured using Endothelial Cell Growth Media plus supplement (without vascular endothelial growth factor [VEGF]) (R&D Systems, Minneapolis, MN). Adipose-derived stem cells (ADSCs) were cultured using MEM Alpha (1X) manufactured by Gibco™ supplemented with 16% FBS and 1% L-glutamine. Co-culture media was prepared by combining Basal Cell Culture Liquid Media DMEM/F12 (Corning, Corning, NY) (50:50 mix) with endothelial cell growth supplement and 10% FBS. All combined media and supplement were vacuum-filtered using a Corning Disposable Vacuum Filter (0.2 µm pore size)/Storage systems prior to usage. Cells were grown at 37 °C in a 5% CO_2 incubator. Media was changed every 48 hours and when confluent, cells were passaged using 0.05% Trypsin-EDTA (1X), phenol red (Gibco™). To quantify cell density, a 1:1 dilution of cell mixture to Trypan Blue Solution, 0.4% (Gibco™) was prepared and transferred to a hemocytometer/counting chamber for

automated counting using the Corning® Cell Counter. Based on cell density, cells were seeded in 12- or 6-well plates at 0.8 x 10^5 cells per well or 1.5 x 10^5 cells per well for downstream transfections or treatments as needed. HUVECs were experimentally treated or transfected at passages 3-5, since after seven passages cells are more susceptible to senescence. ADSCs were also used at a similar passage number range.

In vitro miRNA Transfections

To increase miR-449a expression *in vitro*, miR-449a-5p miRIDIAN microRNA Mimic (Dharmacon™, Lafayette, CO) was diluted to a concentration of 20 nM per well in serum-free media, combined with Qiagen's HiPerFect transfection reagent, and incubated for 10 minutes for enhanced transfection efficiency. Cells were then incubated with the prepared transfection mixture for 3 hours at 37 °C in a 5% CO_2 incubator prior to adding sufficient supplemented media for continued growth. To inhibit miR-449a expression *in vitro*, miR-449a 50 nmol miRIDIAN hairpin inhibitor (Dharmacon™) was diluted to a concentration of 25 nM per well in serum-free media and HiPerFect transfection reagent as described above. Transfections were maintained for a total of 72 hours prior to change of media or whole cell lysate collection using Invitrogen™ TRIzol™ Reagent (ThermoFisher Scientific, Waltham, MA). RNA was isolated through chloroform and ethanol precipitation followed by nucleic acid quantification using the Epoch Gen5 plate reader (BioTek, Winooski, VT). Inhibitor and mimic dosages were determined based on titrated transfection concentrations conducted in our lab.

In vitro Growth Hormone (GH) Administration

GH was prepared by diluting somatotropin (Reporcin, Alpharma, Inc.; Victoria, Australia) in RNAse-free water. To determine the ideal concentration of GH to administer *in vitro*, a cell viability assay was conducted using the CellTiter 96® AQueous One Solution Cell Proliferation

Assay (MTS) produced by Promega (Madison, WI). MTS assays revealed that 5 nM of GH affected viability without promoting cytoxicity and subsequent cell death (Supplementary Figure 4B). Hence, we used 5 nM of GH for the current studies. To ensure GH administration stimulated the affiliated signaling pathway, Pi3K expression was quantified at 6 and 24 hours following GH exposure using RT-qPCR. At twenty-four hours, Pi3K exhibited a relative 3.5-fold increase in expression, indicating the treatment stimulated a response (Supplementary Figure 4A). GH supplementation was maintained over 10 days with miR-449a mimic and inhibitor transfections at Day 2 and Day 7. Whole cell lysates were collected at day 10; miR-449a, $p16^{Irk4a}$, $p21^{Cip1}$, *Ccnd1*, *Pi3K, mTOR*, and *Foxo1* levels were measured with RT-qPCR following RNA extraction (see Supplementary Table 4 for primer sequences).

***In vitro* Co-cultures**

HUVECs were cultured with GH treatment for 5 days and then co-cultured with transfected (20 nM) and non-transfected ADSCs for another 5 days with GH supplementation. CELL TREAT Scientific Products (Pepperell, MA) Permeable Cell Culture Inserts (3.0 μm) were used for co-cultures. Transfected and non-transfected ADSCs were seeded on permeable inserts following 72 hours of transfection time and then transferred to 6-well plates containing GH-treated HUVECs. Following treatment, whole cell lysates were collected from HUVECs and RNA was isolated followed by RT-qPCR. To isolate extracellular vesicles suspended in concentrated conditioned media, media was collected from transfected and non-transfected ADSCs and filtered using Vivaspin centrifugal concentrators optimized for ultrafiltration (Sartorius, Göttingen, Germany). The media was then subject to lysis and RNA isolation, as described in 4.7., followed by cDNA preparation and RT-qPCR (Supplementary Figure 7).

cDNA synthesis and Quantitative Real-Time PCR (RT-qPCR)

Following RNA extraction, cDNA was synthesized using the Applied Biosystems™ TaqMan™ Advanced miRNA cDNA Synthesis Kit (ThermoFisher Scientific) and the iScript™ cDNA Synthesis Kit (Bio-Rad, Carlsbad, CA) for miRNA and mRNA analysis, respectively. Each reaction step was then performed using the Bio-Rad Thermal Cycler T100 according to the manufacturers' protocols. After completing the final step in the Applied Biosystems™ TaqMan™ Advanced miRNA cDNA Synthesis Kit protocol, 10 µL of the final product (50 µL) was diluted in 90 µL of RNase-free water to narrow the range of the control miRNA-16 cycle threshold (C_T) values with RT-qPCR. 2.5 µL of diluted cDNA per sample was then combined with 7.5 µL of the TaqMan Fast Advanced Master Mix and TaqMan miRNA assay for a sample total of 10 µL per well. RT-qPCR was then performed for each sample in duplicate using the QuantStudio 7 Flex Real-Time PCR system to quantify expression of miRNA-16 and miRNA-449a, respectively, using the 477860_mir hsa-miR-16-5p miRNA Assay and 478561_mir hsa-miR-449a miRNA Assay. Following cDNA synthesis using the iScript cDNA synthesis kit, samples were diluted 1:5 for downstream PCR application. To quantify the $p16^{Irk4a}$, $p21^{Cip1}$, *p53*, *Ccnd1*, *Pi3k*, *mTOR*, and *Foxo1*, customized forward and reverse primers designed for each respective gene were provided by Integrated DNA Technologies (Coralville, IA) (see Supplementary Table 4). To prepare each sample for RT-qPCR, Applied Biosystems™ Fast SYBR™ Green Master Mix was combined with the appropriate forward and reverse primer and diluted in nuclease-free water to achieve a total of 18 µL per sample combined with 2 µL of cDNA. RT-qPCR was then performed with two replicates per sample using the Quant Studio 7 Flex Real-Time PCR system. PCR was performed using the MicroAmp™ Fast Optical 96-Well Reaction Plate with Barcode, 0.1 mL and Adhesive PCR Plate Seals (ThermoFisher Scientific) compatible with the Quant Studio 7 Flex Real-Time PCR system.

RT-qPCR data evaluating microRNA differential expression was normalized using miR-16 as the housekeeping gene. When CT values of miR16 had a maximum range of 3 between all samples, the relative expression of miR-449a was calculated using the 2-ΔΔCT method wherein –ΔΔCT denotes the change in CT of the gene of interest normalized to the change in CT of the housekeeping gene. The relative expression of each group was then normalized to the normal/untreated control group by dividing by the average of the control group. As such, the fold-change of expression for miR-449a in all samples can be compared to the control group. RT-qPCR data evaluating mRNA differential gene expression was normalized using β-2 microglobulin (B2M) as the housekeeping gene. When CT values of B2M had a maximum range of 3 between all samples, the relative expression of each gene was then calculated using the 2-ΔΔCT method explained previously. Hence, the fold-change of expression for all genes of interest were normalized to the control group.

Statistical Analysis

All results are presented as mean ± standard error of the mean (SEM). Statistical analysis was conducted using the GraphPad Prism 9.1.0 (221) software via One-Way ANOVA with multiple comparisons (Tukey's test) or independent t-test (if comparing 2 groups). A p-value < 0.05 were considered statistically different.

Single-Nucleus RNA-Sequencing Analysis

After sequencing, the bcl2 files were used to generate the single nuclei matrices by cellranger [49] (10X Genomics), with mapping to the mouse genome (mm10). The analysis pipeline was built up based on a previous report [50]. Briefly, the matrix files from cellranger were used as input for pre-processing and merging steps before being imported into the Seurat package (version 3.1) in R (version 4.1) [51].The genes detected in at least three cells and cells where at least 200 genes

were detected were included in the Seurat analysis. For initial quality control filtering, we selectively removed cells with more than 15% mitochondrial RNA, under 200 detected genes, or above 6,000 genes. Next, the data were log-normalized with a scale factor of 10^4. For visualization and clustering, the initial top 2,000 most highly variable genes were selected and principal components analysis, Harmony [52], and uniform manifold approximation and projection were used as the dimensional reduction technique to construct the clustering graph in Seurat [53]. We identified markers specific to each cluster and calculated differences in expression using the default parameters and the bimodal model [54]. For differential expression genes analysis, we used limmar [55] package to test for differential expression genes and removed genes expressed in less than 10% of the nuclei in both conditions. The genes that were significantly regulated in the same direction in both replicates were included. Cluster Profiler [56] and WikiPathways [57] packages were used for pathway analyses. The cell trajectory inference was performed by decomposing the harmonized PCs in PHATE [58] The ElPiGraph [59] package was used for fitting an elastic principal tree to the PHATE coordinates.

RNA Sequencing Analysis

An average 42,616,251 reads per sample were obtained; of these, 87.04% were aligned to the mouse genome. Principal components analyses of the 500 most variable genes (Supplementary Figure 4A) and unsupervised hierarchical clustering for the top 200 expressed genes (Supplementary Figure 4B) were used to observe and determine variability based on genotype. Based on these findings, sample S17 appeared to be an outlier. Differential gene expression established on genotype was determined based on fold-change, significance in p-value, and significance in adjusted p-value (false discovery rate).

Results

Ames dwarf mice have more stem cells, progenitor cells, and committed pre-adipocytes and upregulated miR-449a in visceral adipose tissue

To capture both mature adipocytes and progenitors, we applied snRNA-sequencing in vWAT freshly isolated from df/df and N/df control male mice. For each condition, we pooled vWAT from 2 mice prior to snRNA-seq, and four datasets were integrated for further analyses. We identified seven major cell clusters, mesothelial cells, spermatozoa, fibroadipogenic precursor cells (FAPs), endothelial cells, mature adipocytes, immune cells, and some unknown cells (Figure 3). These populations are consistent with published cell populations in mouse epididymal WAT [50] and cell clusters were named accordingly. FAPs were increased in df/df mice, suggesting that vWAT from df/df mice has elevated numbers of stem cells, pre-adipocytes, and progenitor cells (Figure 3B and 3C). Next, to understand the molecular pathway maps of FAPs in df/df mice, five subpopulations were categorized in our dataset, labeled FAP1, FAP2, FAP3, FAP4, and FAP5 (Figure 4A). Comparison with previously published results [60] demonstrated that FAP3 is the committed pre-adipocytes cluster (Supplementary Figure 1). There were more FAP3 committed pre-adipocytes in df/df mice, consistent with increased adipose tissue remodeling (Figure 4B and 4C). This is also consistent with previous findings that df/df mice have healthier adipose tissue and composition [27]. Next, we performed differential expression genes analysis for FAPs between normal and df/df mice. Genes highly expressed in df/df mice were enriched for genes encoding proteins involved in insulin signaling and epidermal growth factor receptor (EGFR) signaling, suggesting that these pathways might play an important role in insulin sensitivity and early differentiation of preadipocytes, respectively (Figure 4D).

To validate differences in cell populations within vWAT of Ames dwarf mice versus normal littermates, vWAT was isolated, subjected to lysis, and analyzed by FACS. Using an antibody cocktail containing adipose stem cell markers anti-CD34, anti-Sca-1, anti-CD117, anti-PDGFR-α and a viability stain (7-AAD), cells were sorted and analyzed based on antibody conjugation (Supplementary Figure 2). Compared to N/df mice, there were significantly higher numbers of PDGFR-α +, Sca-1 +, and CD-34 + cells (ADSC positive markers) in vWAT extracted from df/df mice ($p = 0.0193$, Figure 5A). This suggests df/df mice have a higher percentage of ADSCs. Furthermore, RT-qPCR analysis revealed a significant upregulation of miR-449a in df/df mice compared with N/df mice ($p = 0.0191$, Figure 5B) and specifically in ADSCs compared to adipocytes (N p-value = 0.0069, df/df p –value = 0.0284, Figure 5C). Total RNA-sequencing results identified four miR-449a predicted target genes significantly downregulated in df/df mice, suggesting miR-449a is actively suppressing gene targets in vWAT [31] (Supplementary Table 2).

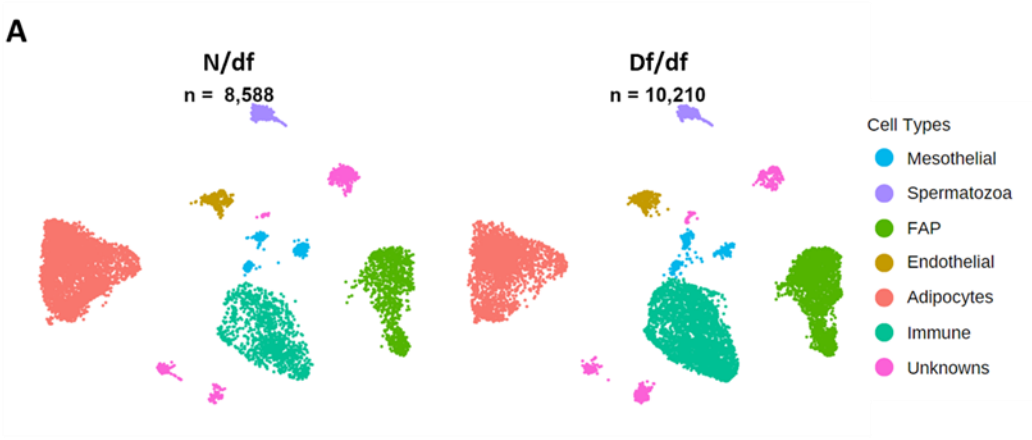

B

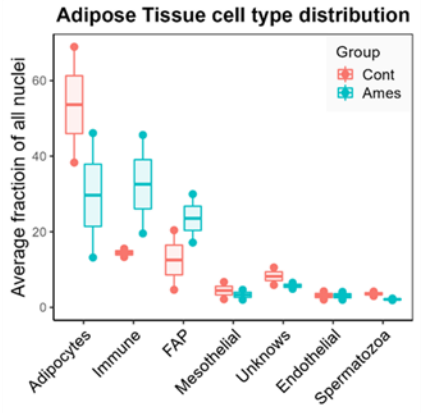

C

Characteristic	Ames, N = 2[1]	Cont, N = 2[1]	p-value[2]
Adipocytes	30 (21, 38)	54 (46, 61)	0.7
Spermatozoa	2.12 (2.01, 2.23)	3.59 (3.29, 3.89)	0.3
FAP	24 (20, 27)	13 (9, 16)	0.7
Unknows	5.70 (5.29, 6.11)	8.24 (7.08, 9.40)	0.7
Immune	33 (26, 39)	14 (14, 15)	0.3
Endothelial	3.06 (2.53, 3.58)	3.15 (2.60, 3.71)	0.7
Mesothelial	3.33 (2.67, 3.98)	4.44 (3.30, 5.58)	0.7

[1] Median (IQR)
[2] Wilcoxon rank sum exact test

Figure 3: Single-nuclei sequencing reveals higher percentage of stem cells, progenitor, and committed preadipocytes in visceral adipose tissue of df/df mice.

A, Different cell populations within visceral adipose tissue distinguished by color. Embedding is based on the 1,000 most variable genes and the first 15 harmonized principle components. Clustering was performed on the UMAP embedding. **B,** Fraction (relative to the total number of nuclei) of each cell type in within visceral adipose tissue of control and df/df mice. **C,** Quantification of cell populations shown in A.

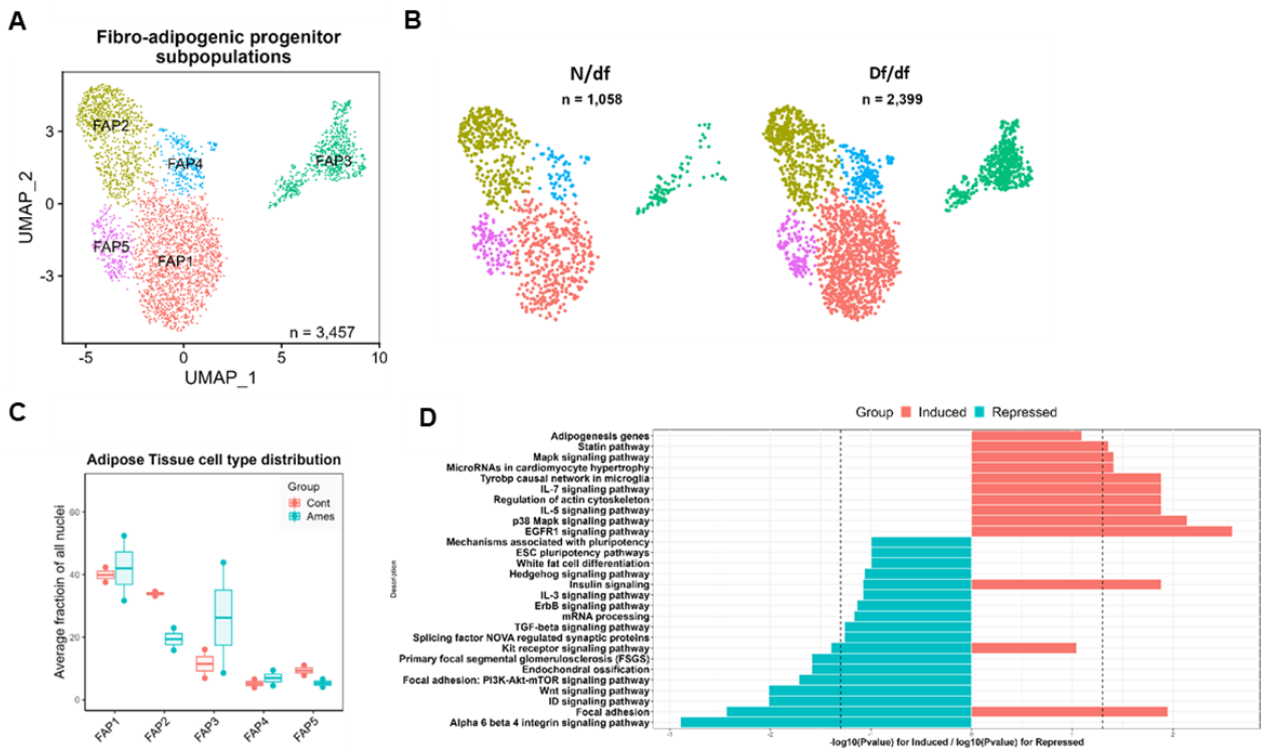

Figure 4: Fibro-adipogenic precursor cells shift towards a preadipocyte phenotype in Ames dwarf mice.

A, figure represents UMAP of FAP subpopulations. The embedding is based on the 2,000 most variable genes and the first 20 harmonized principal components. Clustering was performed based on the UMAP embedding. **B,** UMAPs of FAP subpopulations in control and df/df mice. **C,** Box plot graph showing fraction (relative to the total number of FAP nuclei) of each subpopulation in control and df/df mice. **D,** Levels of the top pathways in Ames Dwarf mice. Dashed line indicates a p value is equal to 0.05.

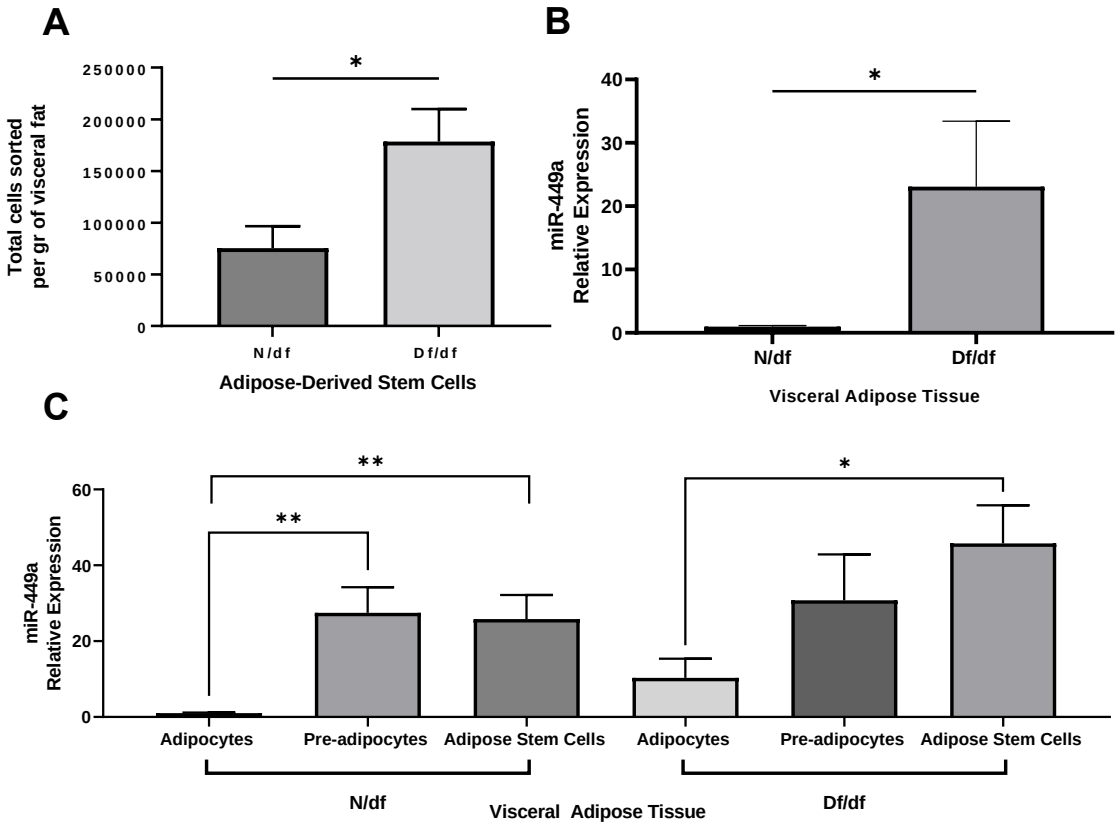

Figure 5: Fluorescence-activated cell sorting revealed higher number of adipose-derived stem cells and qRT-PCR revealed elevated miR-449a in total adipose tissue, adipose-derived stem cells, and preadipocytes isolated from df/df mice versus controls.

A, Total cells sorted per gram of visceral fat gated for live, lineage (-), PDGFRα (+), Sca-1 (+), and CD34 (+) populations. **B**, Relative expression of miR-449a in visceral adipose tissue determined by quantitative RT-PCR. **C**, Relative expression of miR-449a in sorted cells in visceral adipose tissue of N/df and df/df mice. Relative expression was calculated using the $2^{-\Delta\Delta CT}$ method. Statistical analyses used independent t-test (2 groups) or one-way analysis of variance with multiple comparisons (Tukey's test). Values depicted as mean ±SEM. *p-value < 0.05, ** p-value < 0.01, *** p-value < 0.001.

Ames dwarf mice have reduced inflammatory burden and Pi3K-mTOR signaling

snRNA-seq results showed that key pathways associated with immune and inflammatory signaling were repressed in the fibroadipogenic precursor cells (cluster comprising stem cells and progenitor cells). These pathways include TGF-β and interleukin-3 signaling pathways (Figure 4D). RNA-sequencing-derived pathway analyses from total vWAT also identified 14 downregulated and 2 upregulated immune and inflammatory-related pathways (Table 1). Of the 14 downregulated pathways, natural killer cell-mediated cytotoxicity, B-cell receptor signaling, chemokine signaling, T-cell receptor signaling, complement and coagulation cascades, Toll-like receptor signaling, JAK-STAT signaling, proteasome, and regulation of actin cytoskeleton were significantly downregulated in df/df mice. This is consistent with the reduced inflammatory burden in adipose tissue of df/df mice. Additionally, pathways influenced by PI3K-AKT signaling cascades, such as oxidative phosphorylation and JAK-STAT signaling pathways, were significantly downregulated in total vWAT (Table 2) [61]. The VEGF, p53, ErbB, and MAPK signaling pathways were also downregulated. In contrast, insulin signaling was increased in FAPs, suggesting its importance in vWAT remodeling (Figure 4D).

Table 1: Immune and inflammatory-associated pathways regulated in df/df mice compared with N/df mice.

KEGG Pathways	Stat Mean	P-value	Set Size
Immune and Inflammatory-related Pathways			
Natural killer cell-mediated cytotoxicity	-4.629	3.38E-06	97
B cell receptor signaling pathway	-4.027	4.65E-05	74
Chemokine signaling pathway	-3.580	0.000197913	164
T cell receptor signaling pathway	-3.578	0.000216338	104
Complement and coagulation cascades	-3.535	0.000303193	57
Toll-like receptor signaling pathway	-3.366	0.000472863	87
Jak-STAT signaling pathway	-2.696	0.003775438	116
Proteasome	-2.195	0.016317041	42
Regulation of actin cytoskeleton	-1.932	0.027044959	190
Leukocyte transendothelial migration	-1.495	0.068273485	98
Apoptosis	-0.931	0.176853136	82
RIG-I-like receptor signaling pathway	-0.669	0.252875251	51
MAPK signaling pathway	-0.563	0.286913539	237
Ubiquitin-mediated proteolysis	-0.087	0.465482037	132
Calcium signaling pathway	0.747	0.772041938	152
Adipocytokine signaling pathway	1.090	0.861193035	66

Statistical mean refers to statistical distribution of the pattern of differential gene expression in each respective pathway. P-value < 0.05 was considered significant. Set size refers to total differentially expressed genes per pathway.

Table 2: Pi3k-AKT signaling-associated pathways downregulated in df/df mice compared with N/df mice

KEGG pathways	Stat Mean	P-value	Set Size
Pi3k-Akt associated signaling pathways			
Oxidative phosphorylation	-4.31	0.000011	144
B-cell receptor signaling pathway	-4.03	0.000046	74
Chemokine signaling pathway	-3.58	0.00020	164
Toll-like receptor signaling pathway	-3.37	0.00047	87
Jak-STAT signaling pathway	-2.70	0.00378	116
VEGF signaling pathway	-1.48	0.07113	66
p53 signaling pathway	-0.79	0.21667	63
Glycolysis/gluconeogenesis	-0.65	0.25825	52
ErbB signaling pathway	-0.59	0.27654	85
MAPK signaling pathway	-0.56	0.28691	237
Focal adhesion	-0.36	0.35928	190
Cell cycle	-0.19	0.42360	119
mTOR signaling pathway	0.06	0.52552	49
Insulin signaling pathway	1.22	0.88771	129

Statistical distribution of the pattern of differential gene expression in each respective pathway. P-value < 0.05 was considered significant. Set size refers to total differentially expressed genes per pathway.

Senescence-associated genes are differentially expressed in long-living Ames Dwarf mice

To determine if long-living df/df mice as less susceptible to senescence burden [19], RNA was extracted from visceral fat of df/df mice and N/df mice and analyzed for RNA sequencing. We identified 10 differentially expressed genes in df/df mice associated with the senescence phenotype (Table 3). Of these genes, *Ksr2, Hla-g, Cdkn2a (p16^{Irk4a}), Fos, Galectin-3,* and *Pai-1* are linked with inducing or promoting senescence when upregulated [32]. These genes were significantly downregulated in df/df mice compared to N/df littermates. Further, genes typically associated with anti-senescence activity (including *Pdzd2, Arg-Bp2, Vegf-a, Notch3,* and *Bcl6b*) were significantly upregulated in df/df mice. These results suggest that GH-deficient df/df mice are less susceptible to both senescent cell burden and inflammation.

Table 3: Senescence-associated differentially expressed genes in df/df mice vs N/df mice.

Senescence-Associated Differentially Expressed Genes			
Gene name	**Fold change**	**P-value[2]**	**False discovery rate**
Downregulated			
Ksr2	0.2261	0.0000281	0.005
Hla-g	0.3069	0.0047386	0.073
p16	0.3551	0.0000034	0.002
Fos	0.3615	0.0000346	0.006
Galectin-3	0.3992	0.0001805	0.014
Pai-1	0.4415	0.0024224	0.051
Upregulated			
Pdzd2	2.0785	0.000346255	0.019
Arg-bp2	2.1432	0.000001410	0.001
Vegf-a	2.2017	0.000057900	0.007
Notch3	2.3197	0.000000003	0.000
Bcl6b	2.5575	0.000000483	0.001

Genes were cross-references with CellAge Senescence Database [32]. P-value and false discovery rates <0.05 were considered significant.

Statistical distribution of the pattern of differential gene expression in each respective pathway. P-value < 0.05 was considered significant. Set size refers to total differentially expressed genes per pathway.

miR-449a regulates the senescence pathway under senescence-inducing conditions

In HUVECs cultured under normal conditions with RNA isolated at different passages (3, 5, 7, and 13), levels of miR-449a decreased as HUVECs were sequentially passaged. At passage 13, there was no detectable miR-449a expression (Figure 6A). To determine whether miR-449a regulates cellular senescence, $p21^{Cip1}$ and *p53* mRNA transcript levels were quantified in conjunction with senescence-associated β-galactosidase staining in HUVECs transfected with either a miR-449a mimic or inhibitor. Inhibition of miR-449a was associated with increased expression of $p21^{Cip1}$ compared to controls, whereas p53 levels were significantly increased in the miR-449a inhibitor group compared with mimic transfected cells (Figure 6B, 6C) ($p = 0.0263$). Percentages of β-galactosidase-positive cells in the miR-449a inhibitor group significantly increased, suggesting that inhibiting miR-449a promotes a marked increase in senescent cells ($p = 0.0036$; Figure 7A). These results suggest miR-449a suppresses the onset of senescence.

In GH-treated cells, miR-449a levels were significantly downregulated, suggesting that GH has a regulatory role in modulating miR-449a levels ($p = 0.0013$; Figure 6D). To evaluate this result further, HUVECs were subjected to GH and transfected with miR-449a mimic and inhibitor during exposure. Inhibition of miR-449a activity increased both $p16^{Irk4a}$ and $p21^{Cip1}$ levels *in vitro* ($p = 0.0048$ and <0.0001, respectively) (Figures 8A, 8B). These findings are further validated by the increased percentage of SA-βgal+ cells in both the inhibitor and control groups ($p = 0.0013$ and 0.0002, respectively; Figure 7A). Further, overexpression of miR-449a under GH exposure significantly reduced the senescent profile of cells in the control and inhibitor groups ($p = 0.0343$

and 0.0038, respectively; Figure 7B). Hence, miR-449a suppressed onset of senescence in response to GH stimulation.

This reduction in senescence onset may be modulated through the PI3K-AKT signaling pathway. Previous studies have linked increased Pi3K and mTOR activity to reduced longevity [62]. Consistent with those results, we found that the PI3K-AKT signaling pathway is regulated by miR-449a overexpression (Figure 8), suggesting that senescence may be hindered through modulation of mTOR and Pi3Ka. In addition, *Foxo1* expression was reduced; this is typically upregulated when PI3K-AKT signaling is downregulated [62]. Increased FOXO1 activity is typically associated with promoting apoptosis [63]; hence, miR-449a could suppress senescence without promoting apoptosis. To confirm this concept, we carried out flow cytometry analysis of apoptosis and cell death in miR-449a mimic and inhibitor transfected HUVECs. As surmised, miR-449a upregulation did not promote apoptosis (Supplementary Figure 5).

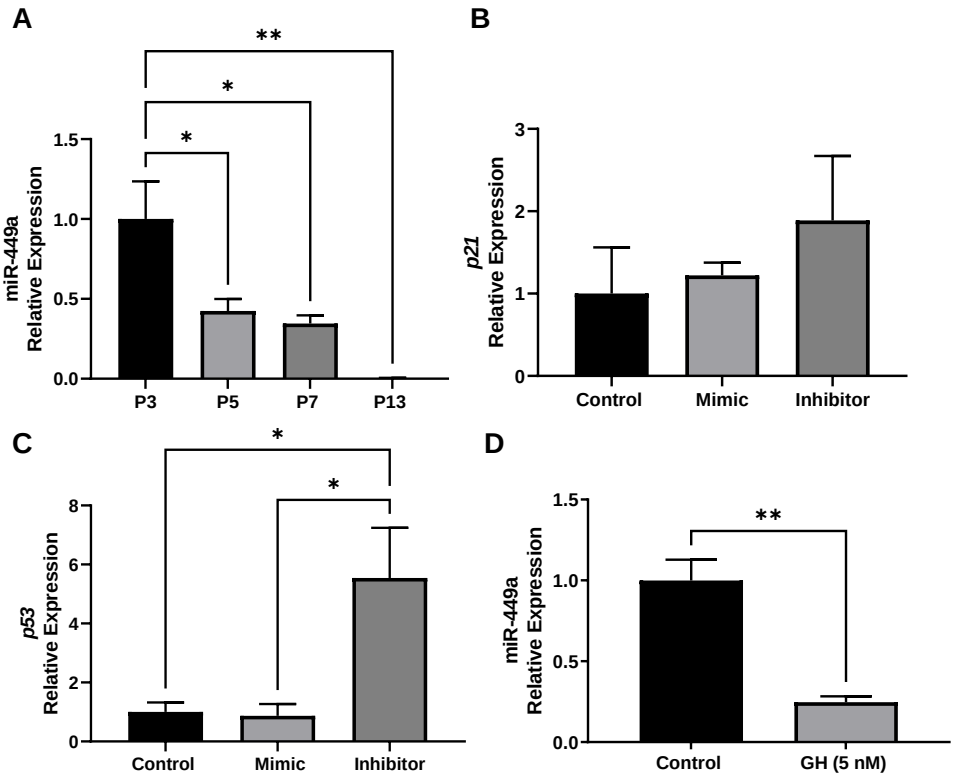

Figure 6: RT-qPCR data reveal that miR-449a is affected by passage number and growth hormone (GH) treatment, and inhibition of miR-449a contributes to increased p21 and p53 expression.

A, Relative expression of miR-449a in HUVECs over four passages. **B and C,** Relative expression of senescence-associated genes *p21* and *p53* in mimic- and inhibitor- transfected cells. **D,** Relative expression of miRNA-449a in GH-treated HUVECs compared with untreated control cells. Relative expression (n = 4 per group) was calculated using the $2^{-\Delta\Delta CT}$ method. Statistical analyses used independent t-test (2 groups) or one-way analysis of variance with multiple comparisons (Tukey's test). Values are mean ±SEM. *p-value < 0.05, ** p-value < 0.01.

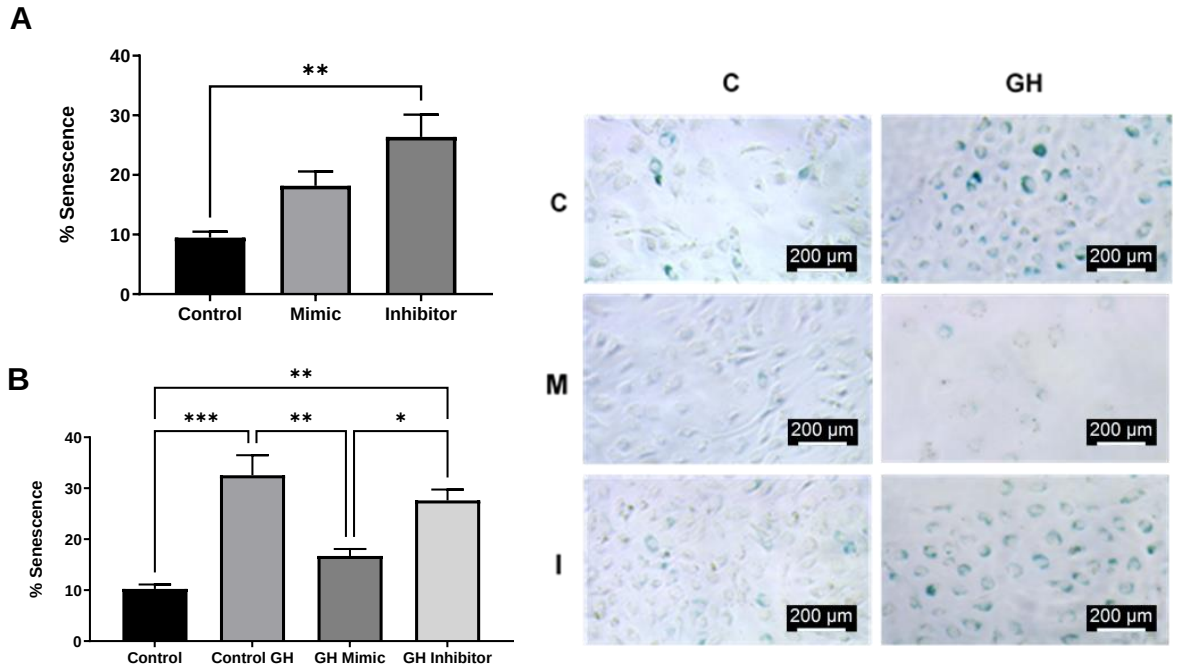

Figure 7: Senescence-associated β-galactosidase activity is suppressed in miR-449a mimic-treated HUVECs.

A, Percentage of senescence-positive cells in control, mimic-transfected, and inhibitor-transfected HUVECs (n = 4 per group). **B,** Percentage of senescence-positive (blue stained) cells in control (C), mimic-transfected (M), and inhibitor-transfected (I) HUVECs treated with 5 nM growth hormone (GH) for 10 days versus untreated controls (n = 4 per group). Blue color is produced in the presence of X-gal and β-galactosidase, wherein the enzyme β-galactosidase (highly expressed in senescent cells) cleaves X-gal to produce the observed blue color. Statistical analyses used one-way analysis of variance with multiple comparisons (Tukey's test). Values are mean ± SEM. *p-value < 0.05, ** p-value < 0.01, *** p-value < 0.001.

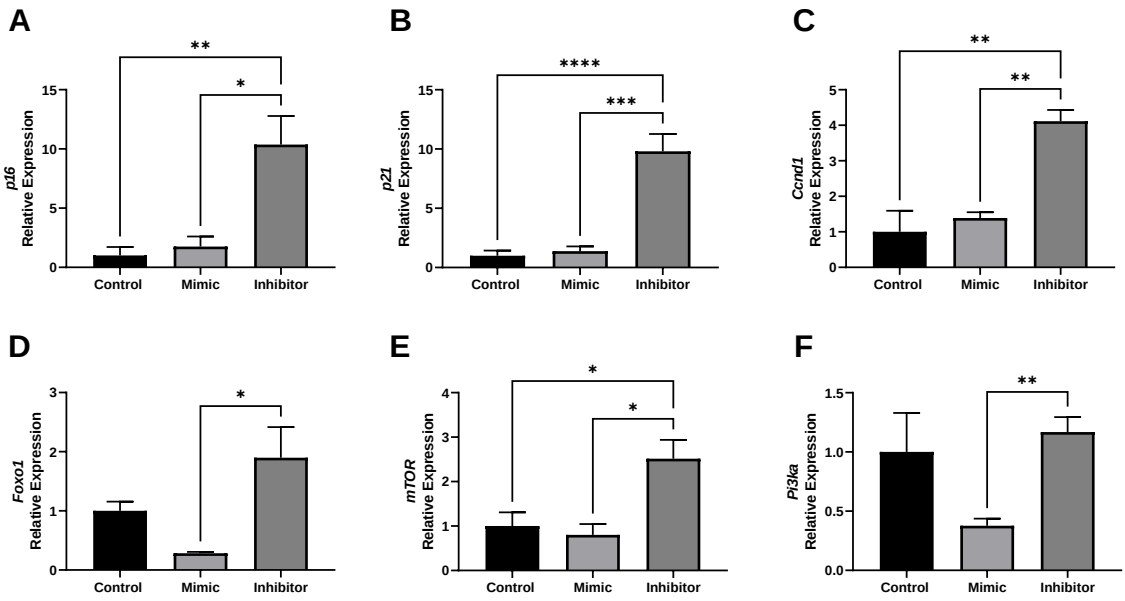

Figure 8: miR-449a regulates pro-senescence genes and modulates the Pi3K-mTOR signaling pathway with growth hormone (GH) treatment.

A-B, Relative expression of senescence markers *p21* and *p16* quantified with real-time PCR in GH-treated and transfected HUVECs. **C,** Relative expression of miR-449a target *Ccnd1* in control, mimic-transfected, and inhibitor-transfected cells. **D,** Relative expression of *Foxo1* in control, mimic-transfected, and inhibitor-transfected cells. **E-F,** Relative expression levels of present *mTOR* and *Pi3ka* with GH treatment. Relative expression (n = 4 per group) was calculated using the $2^{-\Delta\Delta CT}$ method. Statistical analyses used independent t-test (2 groups) or one-way analysis of covariance with multiple comparisons (Tukey's test). Values are mean ± SEM. *p-value < 0.05, ** p-value < 0.01, *** p-value < 0.001, **** p-value < 0.0001.

miR-449a transfected ADSCs promote senescence rescue after induction *in vitro*

To assess the therapeutic potential of miR-449a, HUVECs were cultured under GH treatment (5 nM) for 5 days and then co-cultured with miR-449a transfected (20 nM) and non-transfected (control) ADSCs for an additional 5 days with GH. miR-449a levels increased in HUVECs co-cultured with transfected ADSCs, suggesting miR-449a is being packaged and distributed by these cells ($p = 0.0021$; Figure 9A). In addition, miR-449a levels were significantly increased in exosomes isolated from transfected ADSCs ($p = 0.0392$; Supplementary Figure 6). Further, a reduction in $p21^{Cip1}$ ($p = 0.0325$), *Ccnd1* ($p = 0.0443$) and *Foxo1* ($p = 0.0451$) levels was also observed, with an apparent reduction in PI3K/mTOR signaling (Figure 9B-F). These findings indicate that miR-449a has a robust regulatory role in expression of $p21^{Cip1}$, *Foxo1*, *mTOR*, and *Pi3ka*.

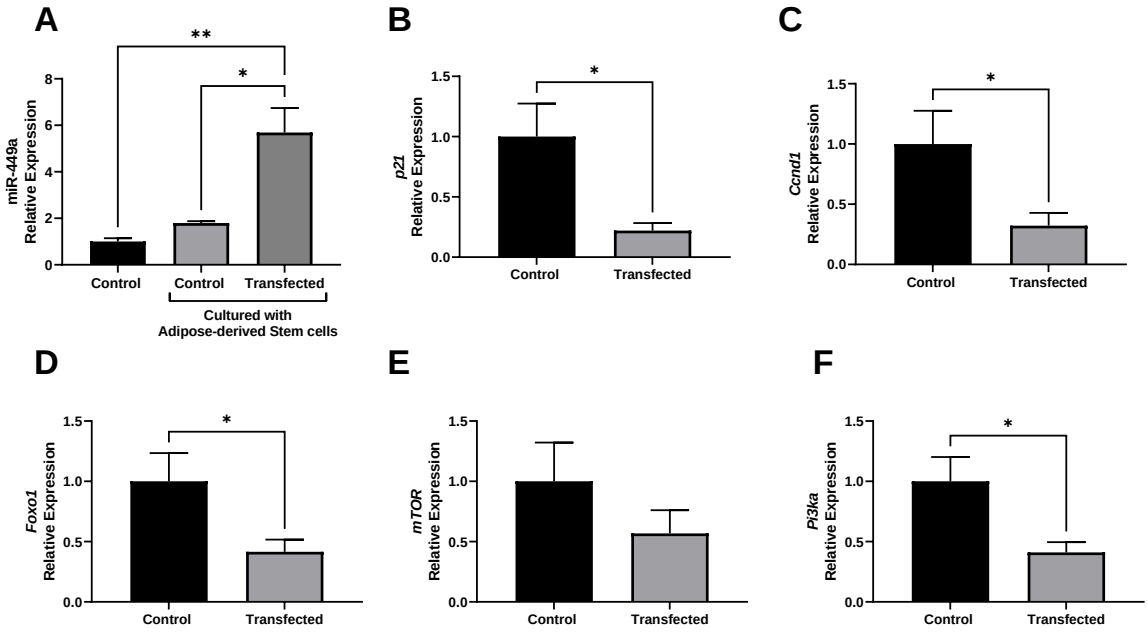

Figure 9: miR-449a uptake in co-cultured HUVECs secreted by adipose-derived stem cells (ADSCs) regulates pro-senescence genes and modulates Pi3K-mTOR signaling with growth hormone (GH) treatment.

A, Relative expression of miR-449a in control HUVECs, HUVECs co-cultured with control ADSCs, and HUVECs co-cultured with transfected ADSCs. **B-F,** Relative expression of *p21, Cyclin D1 (Ccnd1), Foxo1, mTOR,* and *Pi3ka* in GH-treated HUVECs co-cultured with non-transfected ADSCs (control) and transfected ADSCs. Relative expression (n = 4 per group) was calculated using the $2^{-\Delta\Delta CT}$ method. Statistical analyses used independent t-test (2 groups) or one-way analysis of variance with multiple comparisons (Tukey's test). Values are mean ± SEM. *p-value < 0.05, ** p-value < 0.01.

Discussion

Visceral adipose tissue is essential for adaptations in response to metabolic changes within the body. Although snRNA-seq methods have greatly advanced current approaches to understanding the cellular and molecular compositions of tissue, characterization of visceral adipose tissue has not been fully explored. Previously, white adipose tissue was sequenced for identification of cell subtypes in different mouse models. Seven distinct clusters based on gene expression and pathway analysis were identified in epididymal white adipose tissue (eWAT) of DLK1-RFP male mice; five were designated as adipocytes, FAPs, immune cells, endothelial cells, and mesothelial cells. FAPs constitute stem cells, preadipocytes, and fibroblasts. Within these, there are four subpopulations (FAP1, FAP2, FAP3, and FAP4). Based on differential gene expression and pathway analysis, FAP2 is primarily comprised of preadipocytes. Based on these classifications, Sarvari *et al.* compared their clusters to previously identified FAP subpopulations. FAP2 closely resembled ICAM1+ clusters [64], adipose stem cell 1 (ASC1) clusters [65], adipocyte progenitor and committed preadipocyte clusters [60], and P2 progenitor clusters [66]. Although previously identified subpopulations were clustered differently, the FAPs identified were highly similar [50]. In the current study, we clustered the results of single-cell sequencing analyses of vWAT of df/df and N/df (control) mice using a similar approach. We observed that df/df mice have more stem cells/progenitor cells and more committed preadipocytes than N/df mice.

Our findings also suggest that GH-deficient long-living df/df mice exhibit reduced senescence in adipose tissue, likely from the absence of GH. Prior studies have determined that df/df mice have healthier adipose tissue that contributes to their increased lifespan [67]. These findings are consistent with our total RNA and snRNA-sequencing results, which revealed that

GH-deficient df/df mice have altered adipose composition and fewer markers of senescence, senescence-associated secretory phenotype (SASP), and inflammation. Additionally, our findings support the hypothesis that adipose remodeling is increased in df/df mice, exhibited by their greater transition between preadipocytes/progenitor cells to adipocytes. This increase in adipocyte production may contribute to their altered adipose composition and associated health benefits. These results are also consistent with a previous report showing that the absence of GH action resulted in delayed age-related senescent cell (SnC) accumulation and downregulated expression of prominent senescent markers ($p16^{Irk4a}$ and $p21^{Cip1}$) in adipose tissue [45].

Various studies have attributed the reduced senescent burden in df/df mice to altered adipose tissue function [19]. Our results suggest a potential link between reduced expression of pro-senescence genes and inflammatory and PI3K-AKT and mTOR signaling pathways. Previous studies have associated increased mTOR activation with replicative cell senescence. Rapamycin, an mTOR inhibitor, blocks mTORC1 activity and has been used to treat diseases related to aging such as cancer, diabetes, and obesity [68]; it also promotes increased longevity in animal models of aging [69]. GH signaling activates mTOR through PI3K-AKT signaling [10], which then activates MAPK signaling pathways. Reduced AKT activity is associated with reduced cellular senescence and improved longevity [70]. Thus, the lower senescent burden observed in GH-deficient df/df mice may be attributed to increased regulation of the PI3K-AKT signaling pathway in vWAT. Our analysis of visceral adipose content in df/df mice revealed elevated levels of ADSCs, a cell type that confers resistance to oxidative stress-induced senescence and increases angiogenesis [71].

Long-living df/df mice also expressed higher levels of miR-449a in both total vWAT and in ADSCs. These findings are further validated by our previous analysis of circulating miRNAs in

df/df and N/df mice, wherein miR-449a expression decreased with normal aging but was consistent in df/df mice with age [30]. miR-449a regulates the differentiation of mesenchymal stem cells [72] and has previously been implicated in promoting senescence in cancer or tumor cell lines [73]. However, based on our findings, miR-449a is associated with the opposite phenotype in non-cancer cell lines, reducing senescence in HUVECs. In addition, treatment with GH reduces miR-449a levels in HUVECs while increasing the percentage of SnCs.

When we quantified the expression of miR-449a in s HUVECs over 13 passages, miR-449a expression decreased with higher passage numbers. Previously, in senescence accelerated mouse prone 8 (SAMP8) mice, miR-449a levels were significantly reduced with age, but in senescence accelerated mouse resistance 1 (SAMR1) mice, miR-449a levels remained unchanged [33]. These findings support the associations between age and miR-449a and senescence and miR-449a.

In HUVECs treated with GH for an extended period, we found that senescence increased in the GH-treated group and the miR-449a inhibitor-transfected group. However, HUVECs transfected with a miR-449a mimic were rescued from the senescent burden and miR-449a upregulation reduced senescence comparable to untreated controls, once again reinforcing the hypothesis that miR-449a expression is necessary for regulating senescence. Expression of $p16^{Irk4a}$ and $p21^{Cip1}$ was significantly increased in the miR-449a inhibitor transfected group, further confirming the senescent profile.

As a control for the function of the miR-449a inhibitor, *Cyclin D1*, a target of miR-449a, was quantified through RT-qPCR and was increased in the inhibitor group [31]. Although the control group did not exhibit increased $p16^{Irk4a}$ and $p21^{Cip1}$ expression at the mRNA level, β-galactosidase activity was increased in both the control and inhibitor groups, suggesting

senescence is indeed increased by GH treatment. In addition, miR-449a upregulation appears to regulate the expression of *Pi3ka,* suggesting the PI3K-AKT pathway is modulated under GH treatment. This is complemented by a marked increase in *mTOR* expression in the inhibitor group, suggesting miR-449a inhibition results in altered expression of *mTOR* under GH treatment. While *Foxo1* expression was also modulated, this may be attributed to a negative regulation of apoptosis typically promoted by increased FOXO1 expression [63]. Hence, miR-449a may inhibit senescence by regulating *p16/p21* and *Pi3k-mTOR* expression and also regulate apoptosis to ensure cell survival through regulation of *Foxo1*. This notion was validated by our flow cytometry analyses, wherein the percentage of live cell populations were significantly higher in mimic-transfected HUVECs compared to controls. These findings may elucidate how the PI3K-AKT-mTOR signaling in df/df mice is regulated to favor increased lifespan through reduced senescence burden.

Since df/df mice express higher levels of miR-449a and have an increased proportion of adipose-derived MSCs, we aimed to identify the effect of transfecting human ADSCs with miR-449a. Under senescence-inducing conditions promoted by GH exposure, miR-449a levels were increased in HUVECs co-cultured with ADSCs transfected with miR-449a, while $p21^{Cip1}$ levels were downregulated, suggesting miR-449a is reducing senescence. In addition, *Pi3ka* and *mTOR* expression levels were also downregulated by miR-449a, confirming our previous experiments.

ADSCs have been beneficial in reducing age-related pathologies primarily due to their ability to differentiate into different lineages, and have shown therapeutic promise when transfected with miR-449 [74]. Further, ADSCs have improved healing and pain in clinical studies [75]. They are linked to the release of paracrine factors associated with promoting regeneration [76]. Consistent with these earlier reports, preliminary findings from our lab revealed high levels

of miR-449a in extracellular vesicles isolated from transfected ADSCs. Thus, it appears that stem cells can also rescue senescence in GH-treated HUVECs through miR-449a secretion. We also found that levels of *p21^{Cip1}*, *Foxo1, Pi3ka,* and *mTOR* expression levels were downregulated in these conditions, contributing to overall reduced senescence burden and cell survival. These findings suggest a potential therapeutic role of miR-449a in reducing senescence burden through adipose-derived MSCs. Our results also suggest that extracellular vesicles secreted by ADSCs effectively deliver packaged miR-449a to neighboring cells to potentially reduce senescence.

These results suggest that lipid-tagged miR-449a or extracellular vesicles isolated from ADSCs that contain miR-449a could reduce senescence/SASP and improve metabolic health. Overall, our findings support the idea that miR-449a could be used to reduce senescence burden and delay the onset of age-related pathologies associated with cellular senescence.

Conclusion

In summary, our findings support the role of GH in altering adipose tissue composition and the expression of miRNAs that maintain the overall metabolism and health of cells that comprise tissue. In addition, a distinct correlation between GH, aging, and the expression of miR-449a was established. We further demonstrated the functional role of miR-449a in regulating the Pi3K-mTOR pathway that is upregulated in the presence of GH and cellular senescence. Our findings support the prospective use of miR-449a as a senotherapeutic and encourage investigating other miRNAs that exhibit similar potential. Through our functional study with miR-449a, we were interested in investigating the role of miRNAs in a disease model associated with age. As such, we combined the benefits of the Ames dwarf mouse model with an animal model of AD, the APP/PS1 transgenic model. In the corresponding study described in chapter 3, we sequenced miRNAs in the

hippocampi of df/df/APP/PS1, APP/PS1, df/df, and wildtype mice to identify differentially expressed miRNAs that correlate with AD pathology and are affected by the df/df genotype.

CHAPTER THREE: GH DEFICIENCY CONFERS PROTECTIVE ADVANTAGES AGAINST ALZHEIMER'S DISEASE THROUGH A RESCUED MICRORNA PROFILE IN APP/PS1 MICE

Preface

This chapter was previously published as an original article in GeroScience. The article has been reproduced with permission from Springer Nature.

Noureddine, S., Saccon, T., Rudeski-Rohr, T., Gesing, A., Mason, J. B., Schneider, A., Dhabhi, J., Puig, K. L., Rakoczy, S., Brown-Borg, H. M., Masternak, M. M. GH deficiency confers protective advantages against Alzheimer's disease through rescued miRNA expression profile in APP/PS1 mice. GeroScience. 2022 Jul 28. doi: 10.1007/s11357-022-00633-0.

Abstract

Alzheimer's disease (AD) is the most common form of dementia, affecting approximately 6.5 million Americans age 65 or older. AD is characterized by increased cognitive impairment and treatment options available provide minimal disease attenuation. Additionally, diagnostic methods for AD are not conclusive with definitive diagnoses requiring postmortem brain evaluations. Therefore, miRNAs, a class of small, non-coding RNAs, have garnered attention for their ability to regulate a variety of mRNAs and their potential to serve as both therapeutic targets and biomarkers of AD. Several miRNAs have already been implicated with AD and have been found to directly target genes associated with AD pathology. The APP/PS1 mice is an AD model that expresses the human mutated form of the amyloid precursor protein (APP) and presenilin-1 (PS1) genes. In a previous study, it was identified that crossing long-living growth hormone (GH)-deficient Ames dwarf (df/df) mice with APP/PS1 mice provided protection from AD through a reduction in IGF-1, amyloid-β (Aβ) deposition, and gliosis. Hence, we hypothesized that changes in the expression of miRNAs associated with AD mediated such benefits. To test this hypothesis, we sequenced miRNAs in hippocampi of df/df, wild type (+/+), df/+/APP/PS1 (phenotypically normal APP/PS1), and df/df/APP/PS1 mice. Results of this study demonstrated significantly upregulated and downregulated miRNAs between df/df/APP/PS1 and df/+/APP/PS1 mice that suggest the df/df mutation provides protection from AD progression. Additionally, changes in miRNA expression with age were identified in both df/df and wild-type mice as well as df/df/APP/PS1 and APP/PS1 mice, with predictive functional roles in the Pi3k-AKT/mTOR/FOXO pathways potentially contributing to disease pathogenesis.

Introduction

Alzheimer's disease (AD) is the most prevalent form of dementia, affecting an estimated 6.5 million Americans currently [36, 77]. The disease is commonly associated with aging and its course follows a progressive cognitive decline, with early symptoms involving memory loss and later symptoms including personality changes, functional and behavioral impairments that affect the ability to perform daily tasks, and deficits in language function [37]. Unfortunately, the average life expectancy following diagnosis averages 8–10 years, making AD the seventh leading cause of death worldwide [36]. AD pathology is caused by amyloid-β (Aβ) plaque accumulation and hyperphosphorylated tau neurofibrillary tangles in the brain [38]. AD is also linked to increased reactive oxygen species (ROS) production with specific mutations in the amyloid precursor protein (APP) and presenilin-1 (PS1) genes ultimately contributing to APP processing and Aβ deposition [78].

APP/PS1 transgenic mice can be used to model oxidative stress-induced cerebral damage. These mice express the human mutations for APP and PS1 and have been found to exhibit similar outcomes such as increased Aβ and oxidative stress [78]. Meanwhile, Ames dwarf (df/df) mice have been extensively studied for their increased lifespan, which is widely attributed to their associated reduced inflammation, mitochondrial oxidative metabolism and enhanced cellular stress resistance [67, 78]. This increased stress resistance and enhanced longevity is ascribed to the absence of GH and combined loss of pituitary function as a result of the loss of function mutation in their prop-1 gene [70]. In two previous studies, df/df mice were also found to be particularly resistant to Aβ toxicity [78, 79].

To investigate the potential neuroprotective benefits of the hormone deficiencies experienced by df/df mice in AD progression, APP/PS1 transgenic mice were crossed with df/df

mice [78]. This generated the following F2 generations: phenotypically normal mice carrying the dwarf gene (df/+), dwarf mice (df/df), wild type mice (+/+), df/+/APP/PS1 mice, and df/df/APP/PS1 mice. In completing this study, Puig et al. developed a novel mouse model of AD that demonstrated a significant reduction in gliosis, Aβ levels, and IGF-1, suggesting the protective effects associated with GH deficiency in df/df mice can confer advantages for AD pathology as well.

MicroRNAs (miRNAs) have recently garnered attention for their ability to regulate a wide variety of pathways through targeted reduction of the translation of messenger RNAs (mRNAs) [44, 80]. Indeed, several miRNAs have been identified and correlated with AD pathology. For instance, miRNAs-200b, -135a, and -429, regulators of APP and BACE-1 (an enzyme involved in Aβ generation), were shown to be downregulated in the hippocampus of APP/PS1 mice [81]. Other potential miRNAs of interest have also been proposed and experimentally established to be involved in regulating processes crucial to AD outcome. Given the promising findings presented in the study by Puig et al., we were interested in identifying potential biomarkers or changes in expression profiles of miRNAs in the df/df x APP/PS1 crosses. Since AD can be difficult to diagnose, identifying potential biomarkers or factors that are altered with AD could provide added insight into future diagnostics and/or treatment methods. To investigate this, we sequenced miRNAs from hippocampal tissue of df/df, wild type, df/+/APP/PS1, and df/df/APP/PS1 young and old mice.

Materials and Methods

Transgenic Mice and Tissue Collection

For this study, C57BL6/APP/PS1 (APP/PS1; APPswe/PS1dE9; Mo/Hu APPswe PS1dE9; Tg(APPswe,PSEN1dE9)85Dbo) transgenic mice were bred with df/df mice to produce a heterozygous F1 generation that was then bred to produce F2 offspring by Puig et al. [78]. The F2 generation comprised dwarf (df/df), phenotypical normal heterozygous (df/ +), wild type (+ / +), APP/PS1, df/ + /APP/PS1, and df/df/APP/PS1 mice. Mice were genotyped and maintained under controlled light and temperature conditions with food and water provided ad libitum [78]. In this study, the following groups were selected: df/df, wild type, df/ + /APP/PS1, and df/df/APP/PS1 mice. The selected offspring were sacrificed at 3 months of age and 12 months of age for brain collection, hippocampus isolation, and downstream differential microRNA expression analyses (n = 5–6 per group). Harvested tissue was immediately frozen and stored at − 80 °C. All procedures involving animals were reviewed and approved by the UND Institutional Animal Care and Use Committee.

RNA isolation and library prep

Hippocampi collected was cut and weighed to obtain approximately 10 mg of tissue. Samples were lysed and homogenized with QIAzol lysis reagent and zirconium oxide beads (0.5 mm) in a bullet blender. Once homogenized, RNA extraction was achieved using the QIAGEN RNeasy mini kit (Hilden, Germany). All steps were performed in accordance with the provided protocol and total RNA concentrations were measured using the BioTek Epoch microplate spectrophotometer (BioTek, Agilent Technologies, Santa Clara, CA, USA). To prepare libraries for sequencing, 2 µg of total RNA was diluted in RNase-free water and combined with the appropriate NEXTFLEX Small RNA Seq. kit (V3) reagents used in accordance with the manufacturer's protocol (Perkin-

Elmer, Waltham, Massachusetts, USA). All of the samples were purified using the gel-free selection method. Following gel-free selection, libraries were pooled into two separate pools, precipitated using sodium acetate (3 M), ethanol (100%), and glycogen (20 mg/mL), centrifuged, washed with 70% ethanol, and then re-suspended in RNase-free water. The final, concentrated, library pools were then outsourced for QC and Illumina small RNA sequencing.

Statistical analysis

Fold change and relative expression

Alignment and quantification of miRNA libraries was performed using sRNAtoolbox as described before [82]. Statistical analyses of differentially expressed miRNAs was performed using EdgeR [83] on the R software (3.2.2) and miRNAs with a FDR < 0.05 and FC > 2.0 were considered as upregulated, and FDR < 0.05 and FC < 0.50 were considered as downregulated.

Prediction of miRNA target genes and their pathway interactions

DIANA Tool miRPath (v3) was used to generate lists of gene targets and pathways relevant to microRNAs of interest through the micro-T-CDS (V5.0). The DIANA-miRPath v3 was utilized for its ability to provide predicted and experimentally supported miRNA interactions and the pathways they regulate [84]. Alternatively, miRNA gene targets predicted to function in AD pathology were cross-referenced with the miRNA database (miRdb) [31, 85].

Results

Age impacts expression of miRNAs in hippocampi of df/df and wild type (+ / +) mice

To identify changes in miRNA expression with age, we evaluated differentially expressed miRNAs in df/df older mice (12 months of age) in comparison with df/df young mice (3 months of age) as well as in wild-type older mice (12 months of age) in comparison with wild-type young

mice (3 months of age). Results of our analysis revealed downregulated expression of miR-17-5p, miR-19b-3p, miR-22-5p, miR-322-5p, miR-301a-3p, miR-19a-3p, miR-154-5p, miR-337-3p, miR-20a-5p, miR-34a-5p, miR-344b-3p, miR-467d-3p, miR-501-5p, and miR-296-5p in older df/df mice (Table 4). Pathway analysis of these down-regulated miRNAs revealed predicted gene targets involved in MAPK, FoxO, TGF-β, insulin, Pi3K-AKT, mTOR, Ras, and Hippo signaling (Supplementary Table 3). Conversely, miR-148b-5p, miR-1981-5p, miR-744-5p, miR-488-3p, and miR-873a-5p were found to be upregulated in df/df older mice (Table 4). These miRNAs are predicted to regulate genes involved in long-term depression, suggesting these middle-aged df/df mice may be less prone to long-term depression; however, experience increased insulin-signaling and associated pathways with age (Supplementary Tables 3 and 4). Similarly, wild-type older mice exhibited downregulated expression of a set of miRNAs that are also predicted to regulate MAPK, Pi3K-AKT, mTOR, and insulin signaling (Supplementary Table 8). These downregulated miRNAs include miR-296-5p, miR-138–2-3p, miR-669c-5p, miR-1264-5p, miR-204-5p, and miR-let-7c-5p. Both df/df and wild-type mice exhibited significant downregulation of miR-296-5p with age (Table 4). Conversely, miR-375-3p and miR-152-3p were significantly upregulated in older wild-type mice (Table 4). Pathway analysis revealed an association between these miRNAs and Hippo and FoxO signaling pathways, indicating that these two pathways are likely downregulated in these mice (Supplementary Table 7).

Table 4: miRNA expression patterns significantly altered in df/df and wildtype (+/+) older mice compared to young df/df and wildtype mice, respectively.

microRNA ID	+/+	df/df
mmu-miR-17-5p	-	↓
mmu-miR-19b-3p	-	↓
mmu-miR-22-5p	-	↓
mmu-miR-322-5p	-	↓
mmu-miR-301a-3p	-	↓
mmu-miR-19a-3p	-	↓
mmu-miR-154-5p	-	↓
mmu-miR-337-3p	-	↓
mmu-miR-20a-5p	-	↓
mmu-miR-34a-5p	-	↓
mmu-miR-344b-3p	-	↓
mmu-miR-467d-3p	-	↓
mmu-miR-501-5p	-	↓
mmu-miR-296-5p	↓	↓
mmu-miR-148b-5p	-	↑
mmu-miR-1981-5p	-	↑
mmu-miR-744-5p	-	↑
mmu-miR-488-3p	-	↑
mmu-miR-873a-5p	-	↑
mmu-miR-138-2-3p	↓	-
mmu-miR-669c-5p	↓	-
mmu-miR-1264-5p	↓	-
mmu-miR-204-5p	↓	-
mmu-let-7c-5p	↓	-
mmu-miR-375-3p	↑	-
mmu-miR-152-3p	↑	-

p-value and FDR < 0.05 were considered significant (refer to supplementary tables 1 and 2 for statistical values).

miRNAs predicted to regulate the mTOR and FoxO signaling pathways are differentially expressed in df/df/APP/PS1 older mice

Puig et al. previously demonstrated reduced IGF-1 expression in the parietal cortex and hippocampi of df/df/APP/PS1 mice, which is in line with the df/df phenotype, suggesting the absence of GH and other pleiotropic hormones provide advantageous reductions in insulin

signaling that might decelerate brain aging [78]. In our analysis of differentially expressed miRNAs in df/df/APP/PS1 mice compared to wild-type mice, we identified four miRNAs, miR-488a-5p, miR-488-3p, miR-3078-5p, and miR-298-5p, significantly upregulated in the hippocampi of df/df/APP/PS1 mice (Table 5). According to pathway analysis, these miRNAs target mTOR signaling and FoxO signaling (Figures 10 and 11, Supplementary Table 9). Additionally, miR-488-3p may also play a crucial role in regulating onset of long-term depression (Supplementary Table 9). This miRNA was correspondingly upregulated in young df/df mice compared to wild-type young mice (Supplementary Table 10). miR-488-5p and miR-298-5p are also anticipated to regulate endocytosis (Supplementary Table 9) a process implicated in AD pathogenesis through APP and Aβ production [86].

Table 5: miRNA expression patterns significantly altered in df/ + /APP/PS1 and df/df compared to wild-type (+ / +) middle-aged mice as well as df/df/APP/PS1 middle-aged mice compared to df/ + /APP/PS1 middle-aged mice.

microRNA ID	Df/+/APP/PS1	Df/df	Df/df/APP/PS1
mmu-miR-1957a	↓	↑	-
mmu-miR-200b-3p	↓	↓	↑
mmu-miR-488-5p	-	↑	↑
mmu-miR-3078-5p	-	↑	↑
mmu-miR-412-5p	-	↑	↑
mmu-miR-298-5p	↑	↑	↑
mmu-miR-666-5p	-	↑	↑
mmu-miR-488-3p	-	↑	↓
mmu-miR-219b-3p	↑	↓	↓
mmu-miR-219a-5p	↑	↓	-
mmu-miR-29b-3p	↑	↑	↓
mmu-miR-342-5p	↑	↑	-
mmu-let-7b-3p	↑	-	↓
mmu-miR-451a	↑	-	↓
mmu-miR-1b-5p	↑	-	↓
mmu-miR-206-3p	↑	-	↓
mmu-miR-142a-3p	↑	-	↓
mmu-miR-669c-5p	↑	-	↓
mmu-miR-3065-5p	↑	-	↓
mmu-miR-1a-3p	↑	-	↓
mmu-miR-669a-5p	↑	-	↓
mmu-miR-669p-5p	↑	-	↓
mmu-miR-144-3p	↑	-	↓

p value and FDR < 0.05 were considered significant

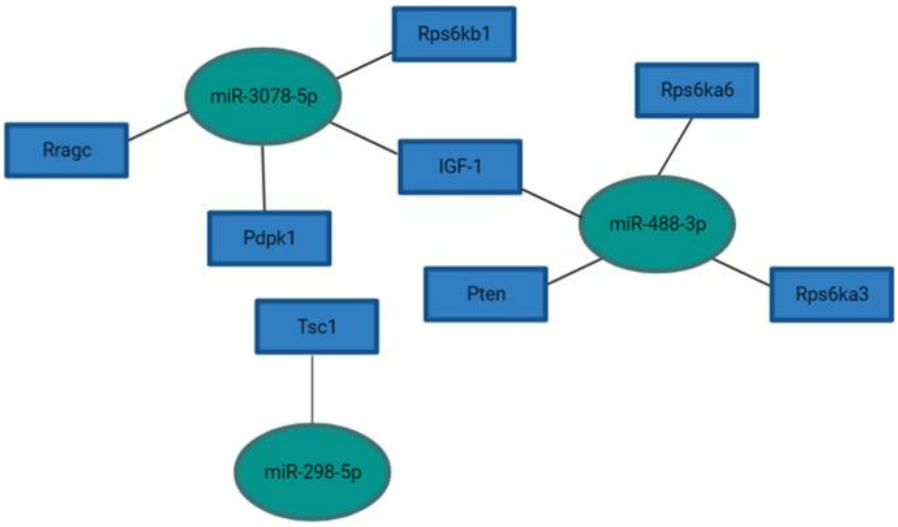

Figure 10: Predicted miRNA interactions with genes implicated in mTOR signaling.

Pathway interactions were derived from DIANA Tools and predicted gene targets were determined using the microT-CDS target prediction algorithm [84]. Refer to supplementary tables 11-13 for differential expression and statistical values for miRNAs selected. Figure was made with BioRender.

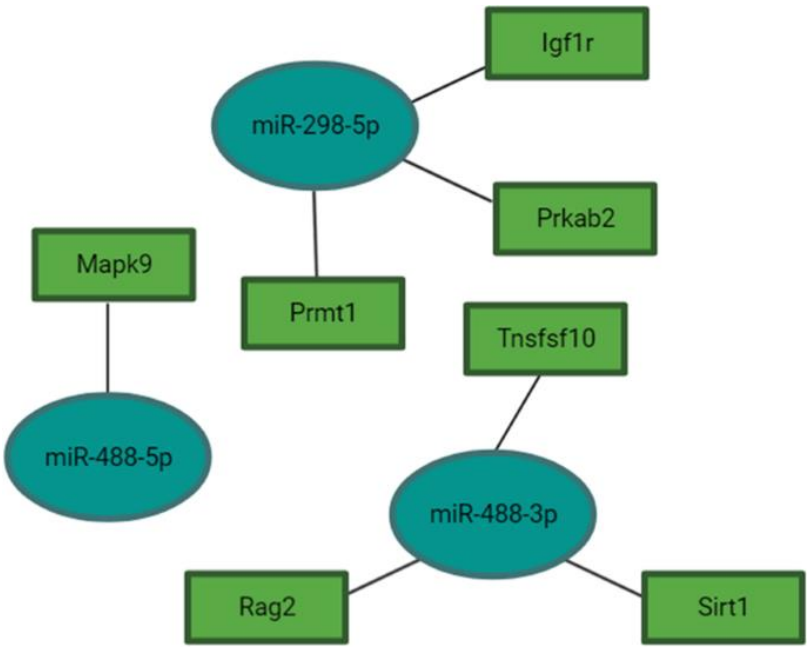

Figure 11: Predicted miRNA interactions with genes implicated in FoxO signaling.

Pathway interactions were derived from DIANA Tools and predicted gene targets were determined using the microT-CDS target prediction algorithm [84]. Refer to supplementary tables 11-13 for differential expression and statistical values for miRNAs selected. Figure was made with BioRender.

miRNAs implicated with AD pathology are differentially expressed in older APP/PS1 mice compared to wild-type mice, as well as in older df/df/APP/PS1 compared to APP/PS1 mice

Several miRNAs have been identified as potential biomarkers or targets of AD. To investigate changes in expression of these miRNAs, we identified miRNAs differentially expressed in df/df, and df/+/APP/PS1 older mice, compared to the wild-type older group, and in df/df/APP/PS1 older mice compared to the df/+/APP/PS1 older mice. The results of this analysis demonstrated upregulated expression of miR-451a, miR-206-3p, miR-144-3p, and miR-142-3p in df/+/APP/PS1 mice with downregulated expression of these miRNAs in df/df/APP/PS1 mice (Table 5). These miRNAs have previously been found to be differentially expressed in APP/PS1

mice and have been linked to increased APP and Aβ levels [87, 88], suggesting that the df/df phenotype may be conferring protection against AD progression through suppression of these miRNAs. The opposite expression profile was observed for miR-200b-3p and miR-219a-5p, which were found to be suppressed in df/df mice but upregulated in df/ + /APP/PS1 mice. Additionally, other miRNAs that may play a crucial role in facilitating AD pathology have also demonstrated similar expression profiles as miR-451a, miR-206-3p, and miR-144-3p. These miRNAs include miR-3065-5p, miR-1a-3p, miR-669a-5p, miR-669p-5p, and let-7b-3p (Table 9). Using the miRNA database (miRdb), we identified predicted gene targets that have been associated with preventing Aβ production through APP facilitation (Figure 12). As such, these miRNAs upregulated in df/ + /APP/PS1 but downregulated in df/df/APP/PS1 mice may serve as novel miRNAs implicated with AD pathogenesis.

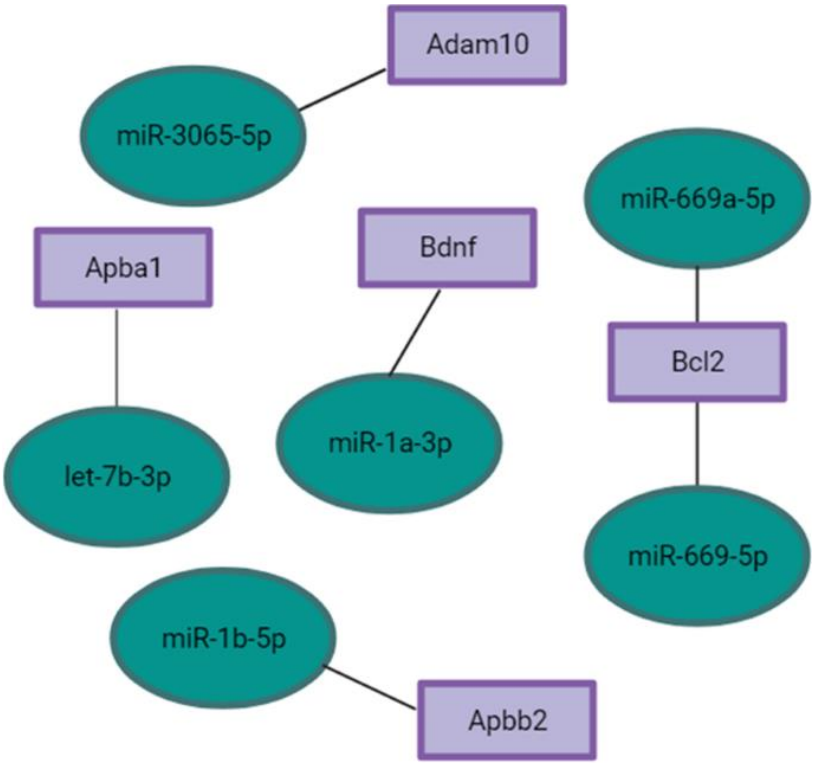

Figure 12: Predicted miRNA interactions with genes implicated in AD pathology.

Genes were cross-referenced with the miRNA database [31, 85]. Refer to supplementary tables 11-13 for differential expression and statistical values for miRNAs selected. Figure was made with BioRender.

Discussion

miRNA sequencing of hippocampal tissue in long-living GH-deficient df/df mice revealed 14 miRNAs downregulated and 5 miRNAs upregulated with age. Collectively, pathway analysis identified predicted gene targets involved in MAPK, FoxO, TGF-β, insulin, Pi3K-AKT, mTOR, Ras, and Hippo signaling pathways that correspond to the expected functional roles of the downregulated miRNAs. On the other hand, miRNAs upregulated with age in df/df mice demonstrated functional potential in regulating genes involved in long-term depression, suggesting df/df mice are less prone to long-term depression, however, demonstrate increased nutrient sensing and insulin-associated signaling in the brain with age. Previous studies have demonstrated a direct association between reduced IGF-1 with increased lifespan. Further, knockouts of insulin receptor substrate 1 (IRS-1), IRS-2, and IGF-1 have led to enhanced lifespan in mice. These findings specifically implicate the PI3k-AKT-mTOR and FoxO signaling pathways in modulating aging [9]. As such, our findings are in line with the literature, since miRNAs predicted to target the aforementioned signaling pathways are downregulated with age. Similarly, wild-type mice had decreased expression of miRNAs predicted to target MAPK, PI3K-AKT, mTOR, and insulin signaling. However, it has been widely established that df/df mice have notably enhanced insulin sensitivity with age when compared with their phenotypically normal littermates. These df/df mice exhibit hypersensitivity to insulin, have low fasting glucose and insulin levels [23], suggesting that GH deficiency and deficiencies in other hormones contribute to their overall improved insulin sensitivity with age and extended lifespan [22], which is also reflected in this study through the regulation of miRNAs in the hippocampi.

Additionally, miR-375-3p and miR-152-3p were significantly upregulated in wild-type mice with age. Pathway analysis revealed an association between these miRNAs and Hippo and

FoxO signaling pathways. FoxO signaling plays a key role in insulin and IGF-1 signaling that is central to metabolic homeostasis [89]. Recent findings have demonstrated an association between dysregulation of FoxO signaling and type II diabetes, which interestingly, has been linked to increased risk of AD pathogenesis. This is likely due to the observed escalation in metabolic dysfunction in the AD brain [89]. Moreover, our findings demonstrated differentially expressed miRNAs that might be upregulated due to the absence of GH in df/df/APP/PS1 mice. These miRNAs include miR-3078-5p, miR-488-3p, miR-488-5p, and miR-298-5p. Pathway analysis demonstrated predicted functional roles for these miRNAs in regulating FoxO and mTOR signaling as well as endocytosis and long-term depression. FoxO and mTOR signaling pathways have been well established to be associated with AD pathogenesis, particularly due to the importance of both in maintaining metabolic homeostasis. Although suppression of FoxO signaling can bear negative impacts on the brain, such as through early depletion of neuronal stem cell pools [90], the genes regulated by these miRNAs are primarily associated with insulin-associated Pi3K-AKT-mTOR signaling as opposed to the broader function of FoxO signaling in maintaining cellular processes. Insulin-associated Pi3K-AKT signaling has widely been implicated with accelerating aging, a phenomenon that has deleterious effects on AD pathology [90, 91].

Furthermore, our findings revealed several mechanisms by which the reduction of Aβ plaque deposition and concentrations of $A\beta_{1-40}$ and $A\beta_{1-42}$ in df/df/APP/PS1 transgenic mice, demonstrated by Puig et al. [78], could be mediated. miR-451a, miR-206-3p, and miR-144-3p were found to be downregulated in df/df/APP/PS1 mice, while significantly upregulated in df/+/APP/PS1 mice, suggesting the absence of GH and the benefits observed in df/df mice may confer advantages for the AD brain. miR-451a and miR-144-3p, miRNAs found to target

ADAM10 and BCL2 as well as KH domain-containing RNA binding protein (QKI), modulate key regulators of Aβ and tau biosynthesis and transport, as well as regulate synaptic function and neuronal apoptosis. These miRNAs were found to be downregulated in APP/PS1 mice at different ages [88]. Correspondingly, our findings demonstrated a similar expression pattern in df/df/APP/PS1 mice; however, we found these miRNAs to be upregulated in df/ + /APP/PS1 mice compared to wild-type mice. Further, studies investigating the role of BCL2 in AD pathogenesis have reported a correlation between reduced BCL2 expression and $A\beta_{1-40}$ levels, citing $A\beta_{1-40}$ downregulates BCL2 expression [92]. BCL2 plays a critical role in regulating neuronal intracellular calcium signaling. Changes in calcium signaling is directly linked to neuronal loss in AD which can lead to attenuation of synapses, a phenomenon that is evident in early disease pathogenesis [93]. As such, downregulations in miR-451a and miR-144-3p may be advantageous for AD pathology. Similarly, miR-206, a miRNA associated with reduced brain-derived neurotrophic factor (BDNF) expression in APP/PS1 mice [87], was also significantly repressed in df/df/APP/PS1 mice, specifically through a reduction in the 3' fragment (miR-206-3p). miR-206-3p is predicted to target BDNF, the most widely expressed neurotrophin in the brain [87]. BDNF functions primarily by regulating neurotransmitter release, neurite outgrowth, long-term potentiation, as well as gene transcription of genes involved in intracellular signaling pathways. In the context of AD, BDNF provides protection against Aβ toxicity [87]. As such, our findings indicate the df/df/APP/PS1 phenotype may be neuroprotective against Aβ toxicity through reduced miR-206-3p expression.

A previous study showed that APPtg and TAUtg mice have increased expression of miR-142a-5p while we demonstrated that df/df/APP/PS1 mice have reduced expression of miR-142a-3p. Human AD brain samples also demonstrate upregulated expression of miR-142a-5p,

suggesting a potential role for this miRNA in AD progression [94]. On the other hand, miR-200b-3p, which belongs to the miR-200b family, has been implicated with regulation of APP and Aβ levels and is downregulated in APP/PS1 mice [81]. Our findings suggest a similar expression pattern in df/ + /APP/PS1 mice, while df/df/APP/PS1 mice exhibited upregulated expression of miR-200b-3p. Similarly, miR-219a-5p, a miRNA upregulated in both df/ + /APP/PS1 mice and in human AD brains [95] was also found to be suppressed in df/df mice. Taken together, it appears the GH deficiency in df/df mice provides protective advantages in AD pathology through the above-mentioned differentially expressed miRNAs. Other miRNAs that potentially play a crucial role in AD pathology were found to be repressed in df/df/APP/PS1 mice but increased in df/ + /APP/PS1 mice as well. These miRNAs include let-7b-3p, miR-3065-5p, miR-1a-3p, miR-669a-5p, and miR-669p-5p. Cross-analysis identified predicted gene targets and potential functional targets in regulating AD pathology [31, 85]. For instance, let-7b-3p is anticipated to target APBA1 (also known as X11α), a suppressor of the production of APP fragments (including Aβ peptides) [96]. Similarly, miR-3065-5p is predicted to target ADAM10, implicated with reducing Aβ production, tau pathology, as well as maintaining synaptic function, neurogenesis, and regulating neuronal networks in the hippocampus [97]. Further, miR-1a-3p is expected to target BDNF, which as described previously, is crucial in regulating AD. miR-669a-5p and miR-669p-5p, on the other hand, are anticipated to target BCL2 [31, 85], which plays a crucial role in regulating intracellular calcium signaling and thereby maintaining neuronal function [93]. With these miRNAs being effectively repressed in df/df/APP/PS1 in comparison to df/ + /APP/PS1, it is apparent that the GH deficiency provides protection from AD.

Conclusion

Overall, our findings provide a strong rationale and basis for the advantages conferred by the GH deficiency in AD progression in APP/PS1 transgenic mice. Our data support several potential mechanisms by which the df/df mutation provides protection against AD, as well as validates the current literature regarding the role of miRNAs in AD advancement. Future considerations include deriving the functional and mechanistic roles of the newly proposed miRNAs that could potentially serve as therapeutic targets in AD.

CHAPTER FOUR: CONCLUSIONS AND FUTURE CONSIDERATIONS

There is great interest in the potential for miRNAs to serve as biomarkers for predicting disease and/or in therapeutics targeting intracellular pathways implicated with aging and age-associated pathologies. Due to the capacity of these small RNAs in regulating gene expression at the post-translation level [28], expression patterns of miRNAs in disease models can provide a wealth of information regarding changes in regulation of specific signaling pathways and proteins that change depending on the severity of disease. Furthermore, studies involving miRNAs as therapeutics show potential in overcoming toxicity and invasiveness of current treatment methods [17, 28]. Hence, our work was largely centered on the role of miRNAs in aging and the age-impacted disorder AD.

Our research has focused on evaluating the mechanistic function of an age-associated miRNA, miR-449a, which demonstrates pro-longevity potential in cellular senescence – a major contributor to the aging phenotype. In doing so, we tested the hypothesis that long-living df/df mice encompass healthier adipose tissue composition that serves as a youthful source of miR-449a, a miRNA we anticipated regulates cellular senescence by targeting senescence-associated genes. miR-449a was found to be steadily expressed in long-living df/df mice, while phenotypically normal mice exhibited reduced expression of this miRNA with age [30]. Our preliminary findings also suggest that this miRNA is highly expressed in stem cells derived from adipose tissue of df/df mice, a notion that likely contributes to their healthier adipose composition. Through single-nuclei sequencing and fluorescence-activated cell sorting of visceral adipose tissue from df/df mice, we identified higher percentages of stem cells, progenitor cells, and committed preadipocytes when compared with adipose tissue isolated from phenotypically normal control mice. These findings suggest df/df mice possess a higher number of undifferentiated cells in their visceral adipose tissue,

a factor that likely contributes to their enhanced longevity since stem cell exhaustion is one of the nine hallmarks of aging that can negatively influence tissue health and lifespan [3]. Furthermore, RT-qPCR analysis of the relative expression of miR-449a within these cell populations revealed significantly elevated expression in adipose-derived stem cells, suggesting a source of steadily expressed, circulating miR-449a in df/df mice with age. Our functional study with this miRNA elucidated its regulatory function in the Pi3K-mTOR signaling pathway, specifically under GH-stimulated senescent conditions. Increased intracellular miR-449a effectively provided senescence-rescue under GH exposure in a human cell line, demonstrating its clinical translational potential for targeting senescence in humans. Our work, outlined in chapter 2, also demonstrated the outcome of inhibiting miR-449a, a miRNA that declines with age in both control mice and in sequentially passaged human cells. Inhibition of miR-449a led to a direct increase in p21 and p16, markers of senescence, and revealed increased β-galactosidase activity, an enzyme expressed primarily in senescent cells.

Although our findings provide strong support for the role of miR-449a in contributing to enhanced adipose composition in df/df mice, reduced onset of senescence, and in targeting the Pi3K-mTOR signaling pathway, a complex model would be required for furthering our understanding of the function of this miRNA. This would entail exploring the role of miR-449a *in vivo* by treating mice with miR-449a mimetics and inhibitors and/or EVs from transfected stem cells to fully elucidate the functional capacity of this miRNA in enhancing lifespan. In addition to treating animals with miR-449a mimetics/inhibitors, it would be beneficial to explore upregulating and inhibiting this miRNA *in vivo* in a senescence model, which can be achieved through diet-induced obesity, radiation exposure, or through an aging model. The experimental conditions imposed *in vivo* could also be expanded to an *in vitro* model utilizing other cell lines and similar

senescence-induction protocols such as high glucose (mimics diet-induced obesity) or radiation, to parallel the findings in the animal model. This would provide a well-rounded functional study for additional investigative insight into the mechanism of miR-449a that would be a great addition to the findings presented in chapter 2. However, despite these considerations for expanding on the work that was presented, our study with miR-449a demonstrated adequate support for its potential to address a current gap in the field pertaining to non-invasive anti-aging therapies.

Based on the functional capability of miR-449a in regulating onset of cellular senescence, we were interested in evaluating changes in miRNA expression patterns in a disease model. Since AD is the most prevalent form of dementia and the seventh leading cause of death globally [36], we explored the effect of GH on miRNAs in AD utilizing the transgenic APP/PS1 mouse model crossed with the Ames dwarf model [78]. The resultant F2 generation comprising df/df, wildtype, df/+/APP/PS1, and df/df/APP/PS1 mice allowed for analysis of differentially expressed miRNAs in the hippocampi of GH-deficient and GH-expressing APP/PS1 mice compared to wildtype and df/df controls. The results of this study revealed downregulation of miRNAs-451a, -206-3p, -142-3p, and 144-3p, previously linked to increased APP and Aβ levels [98] by the df/df phenotype, suggesting GH deficiency may be conferring protection against AD through suppression of these miRNAs. Other differentially expressed miRNAs, miRNAs-3065-5p, -669a-5p, -669c-5p, -1a-3p, and let-7b-3p showed comparable potential for promoting AD progression [31] and were similarly downregulated in the absence of GH. These miRNAs could serve as potential therapeutic targets in AD, however, would require additional investigations into their mechanistic functions in pathways that contribute to AD. Moreover, miRNAs associated with regulating mTOR and FoxO signaling, miRNAs-488-5p, -3078-5p, and -298-5p were upregulated in the absence of GH, suggesting these miRNAs may serve as therapeutics for regulating nutrient sensing [84], which

when deregulated negatively contributes to AD pathology, however, would necessitate additional exploratory studies to fully elucidate their roles in AD. Furthermore, future studies could seek to investigate changes in miRNA expression patterns in different regions of the brain, since our study was centered on the hippocampi – one of three regions of the brain affect by AD.

Overall, the work presented in this dissertation supports the potential of miRNAs to serve as therapeutic agents by targeting and regulating age-related pathways such as cellular senescence – as demonstrated by our functional study utilizing miR-449a. Additionally, miRNAs clearly have the ability to contribute to advancing current therapies but more importantly, demonstrate potential to act as biomarkers for predicting disease, a notion that could greatly advance diagnostic methods in the field of medicine [99]. Our findings moreover emphasize the importance of the long-living df/df mouse model in providing added insight into candidate miRNAs that could be used to study age-related diseases. This is largely attributed to their GH-deficiency and altered miRNA expression profile, as demonstrated in both the miR-449a and AD studies. Hence, the documented findings presented here strongly support the promising roles of miRNAs in aging and age-associated diseases.

APPENDIX: SUPPLEMENTARY FIGURES

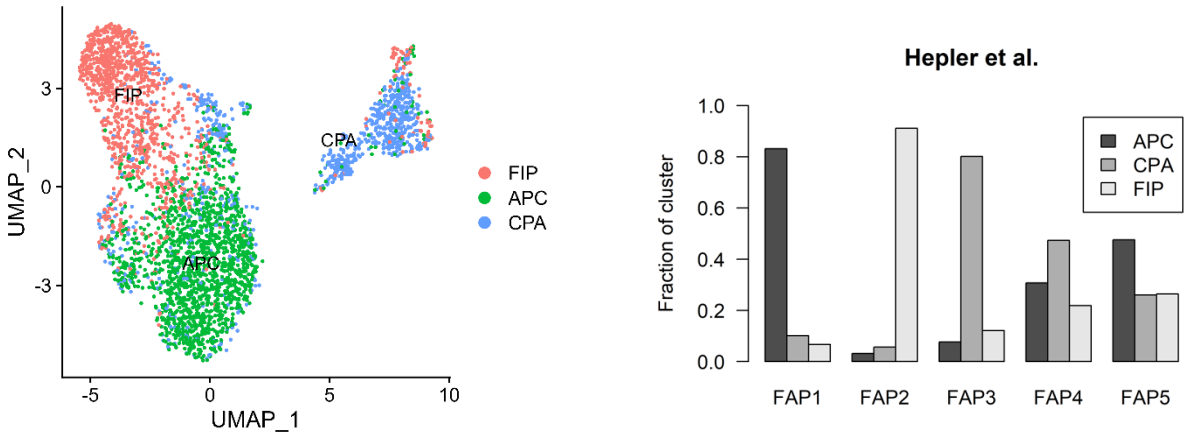

Supplementary Figure 1: Overlap between the identified FAP subpopulations and subpopulations of FAPs defined in Hepler et al.

A list of significantly enriched marker genes of Hepler et al. identified FAP subpopulations were downloaded. Gene module scores in our FAPs were calculated for the downloaded markers and scaled. Each FAP subpopulation were assigned to a previous identified subpopulation according to the module score it most strongly associated with. Left panel: UMAP of FAP nuclei assigned according to previously defined FAP subpopulations. Right panel: The fraction of nuclei in each of the FAP subpopulation assigned to the indicated subpopulations from Hepler et al. study [60].

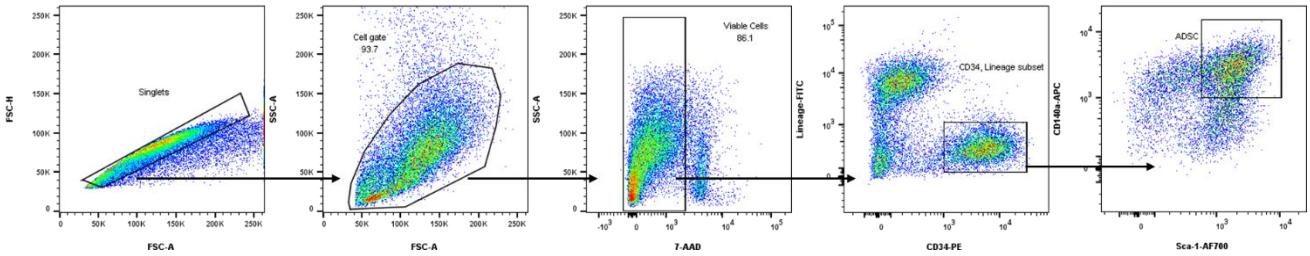

Supplementary Figure 2: FACS gating strategy for sorting ADSCs isolated from visceral adipose tissue of N/df and df/df mice.

Figure depicts method used for gating populations of cells based on antibody conjugation. Cells identified as ADSCs were gated for live, lineage (-), PDGFRα (+), Sca-1 (+), and CD34 (+) populations.

Supplementary Table 1: Forward and reverse primer sequences used in RT-qPCR for gene expression analysis.

Gene	Forward Primer Sequence	Reverse Primer Sequence
B2M	5' GAG TAT GCC TGC CGT 3'	5' CGG CAT CTT CAA ACC TCC AT 3'
p21	5' TGT CCG TCA GAA CCC ATGC 3'	5' AAA GTC GAA GTT CCA TCG CTC 3'
p16 (CDKN2A)	5' CTC GTG CTG ATG CTA CTG AGGA 3'	5' GGT CGG CGC AGT TGG GCT CC 3'
p53	5' CGT GGA AGT GAG AAG TGC TAA A 3'	5' AGA AAT GCA GGC GGA GAA TAG 3'
CCND1	5' TCT ACA CCG ACA ACT CCA TCC G 3'	5' TCT GGC ATT TTG GAG AGG AAGTG 3'
FOXO1	5' CTG GCT CTC ACA GCA ATG AT 3'	5' CAA GAT CAT CCT GTT CGG TC 3'
mTOR	5' ATG CTT GGA ACC GGA CCT G 3'	5' TCT TGA CTC ATC TCT CGG AGT T 3'
Pi3Ka	5' AGT AGG CAA CCG TGA AGA AAA G 3'	5' GAG GTG AAT TGA GGT CCC TAA GA 3'
BCL2	5' CTG CGA ATA CCG GAC TGA AA 3'	5' TCC CAT CAA TCT TCA GCA CTC 3'
BCL2-L11	5' CCA GAT CCC CGC TTT TCA TCT 3'	5' GTT CAG CCT GCC TCA TGG AA 3'

Primers were designed and manufactured through Integrated DNA Technologies.

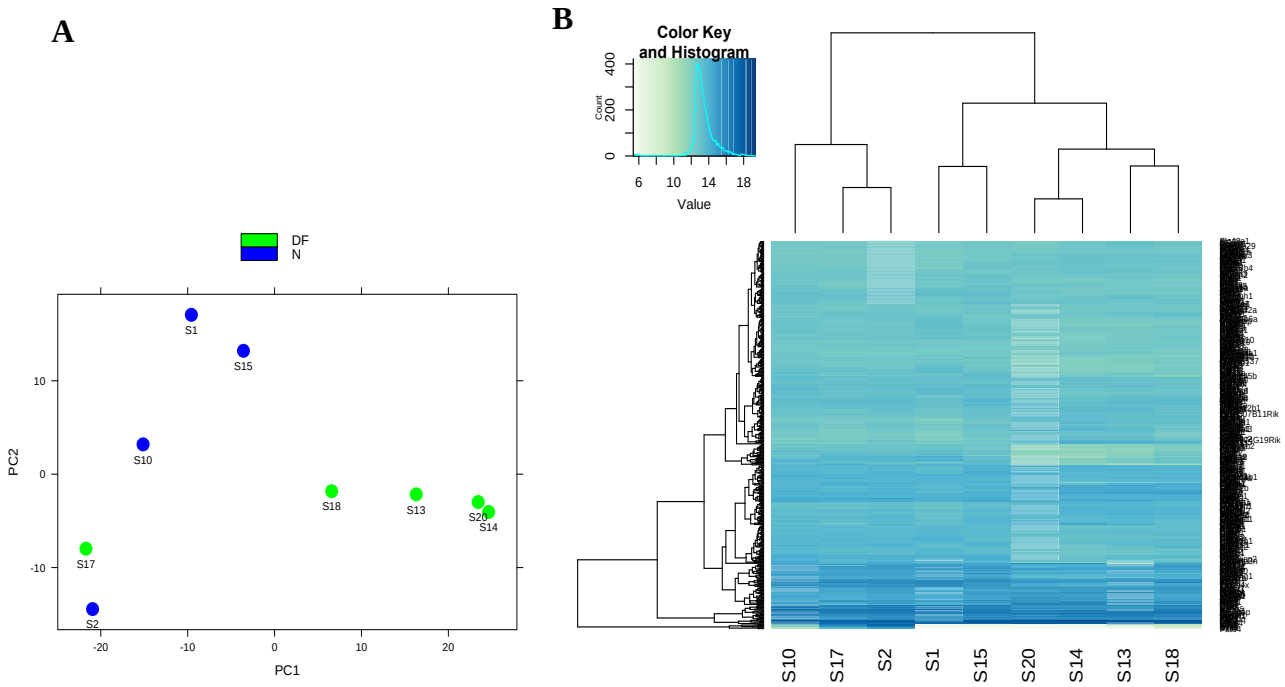

Supplementary Figure 3: Principal component analysis and unsupervised hierarchical clustering for gene expression in df/df and N/df mice.

A, Principle component analysis of the 500 most variable expressed mRNAs in df/df (n = 5; green) and N/df mice (n = 4; blue). **B**, Unsupervised hierarchical clustering expression levels for the top 200 most expressed genes in df/df (S13, S14, S17, S18, and S20; n = 5) and N/df (S1, S2, S10, and S15; n = 4) mice.

Supplementary Table 2: miR-449a targets are downregulated in df/df mice compared to their phenotypically normal littermates

miRdb miR-449a Gene Targets		
Gene name	**FC**	**P-value**
Shisal-1	0.283249	0.001194
Grem-2	0.382704	0.000030
Rnf128	0.403744	0.001389
Bcl2a1a	0.60784	0.040880

Gene targets were identified through the miR-database [31]. FC indicates fold change; FC in expression < 0.5 is considered downregulated, p-value < 0.05 is considered significant.

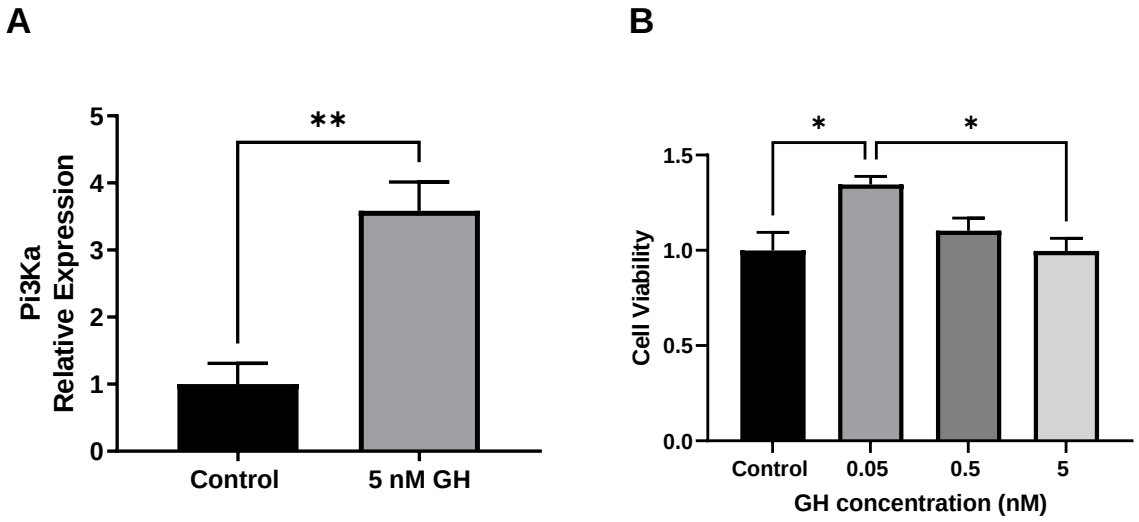

Supplementary Figure 4: 5 nM of GH affects cell viability and stimulates Pi3K expression. **A**, data demonstrates Pi3K expression quantified through RT-qPCR at 6- and 24-hours post-GH exposure compared with the untreated control. **B**, figure presents results of MTS assay on titrated exposure of GH in HUVECs. Cell viability was assessed using a spectrophotometer where

absorbance was recorded at 490 nm. Findings suggest 5 nM of GH to be most effective at stimulating a response in cells. Relative expression (n = 3 per group) was calculated using the $2^{-\Delta\Delta CT}$ method. Statistical analysis was performed using One-Way Anova with Multiple Comparisons (Tukey's test). Values are mean ± SEM. *p-value < 0.05, ** p-value < 0.01, *** p-value < 0.001.

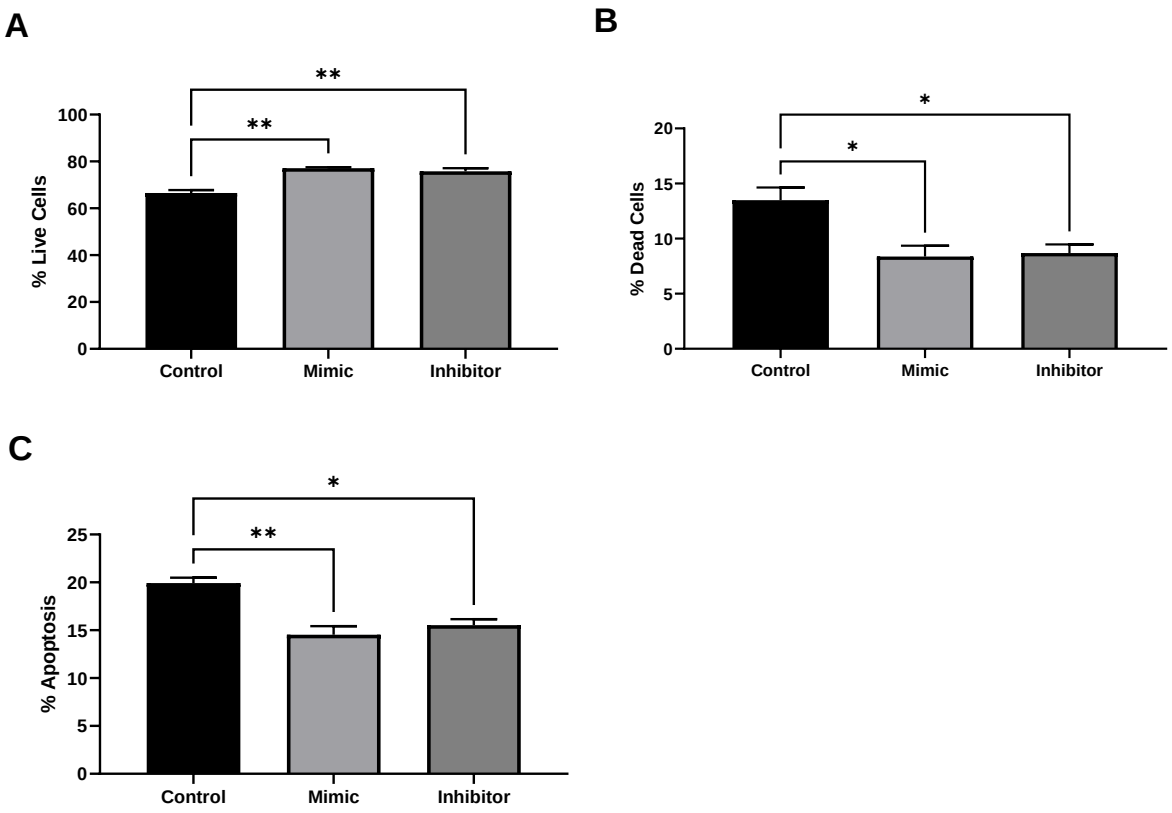

Supplementary Figure 5: miR-449a overexpression does not induce apoptosis in HUVECs transfected with miR-449a mimic.

Flow cytometry analysis of apoptosis and cell death using the Invitrogen™ Dead Cell Apoptosis Kit with Annexin V FITC and PI, for flow cytometry revealed a significant increase in the percentage of live cells in mimic-transfected HUVECs. CytoFLEX S Flow Cytometer by Beckman

Coulter was used to identify live, dead, and apoptotic cell populations in transfected and control HUVECs. Gating was achieved in accordance with the manufacturer's suggestions using the CytoFLEX software wherein live cells demonstrate weak annexin V staining of the cell membrane while apoptotic cells show higher surface labeling. Dead cells demonstrate both membrane staining by annexin V and propidium iodide (nuclear stainng). Downstream statistical analysis was conducted on Excel and GraphPad Prism 8.0. Statistical analysis was performed using One-Way ANOVA with Multiple Comparisons (Tukey's test). Values are mean ± SEM. *p-value < 0.05, **p-value <0.01.

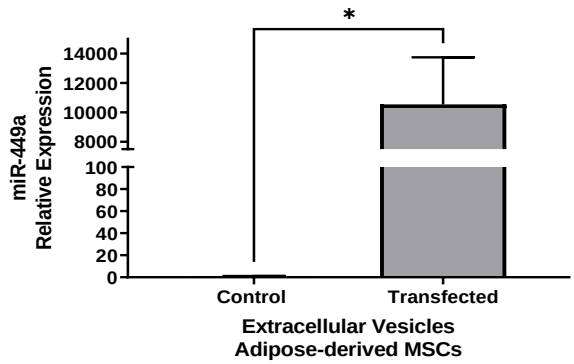

Supplementary Figure 6: Relative expression of miR-449a in extracellular vesicles isolated from transfected and non-transfected (control) adipose-derived stem cells.

Relative expression (n = 3 per group) was calculated using the $2^{-\Delta\Delta CT}$ method. Statistical analysis was performed using independent t-test (2 groups). Values are mean ± SEM. *p-value < 0.05.

Supplementary Table 3: Differentially expressed miRNAs in df/df middle-aged (12-months) mice compared to df/df young (3-months) mice.

Downregulated				
	logFC	logCPM	p-value	FDR
mmu-miR-17-5p	-1.54799	5.896644	3.86E-06	0.000915
mmu-miR-19b-3p	-1.73578	7.259701	1.17E-05	0.001112
mmu-miR-22-5p	-1.26847	7.554657	1.00E-05	0.001112
mmu-miR-322-5p	-1.3508	5.873406	2.18E-05	0.001474
mmu-miR-301a-3p	-1.38349	6.137288	2.92E-05	0.001732
mmu-miR-19a-3p	-2.07278	3.213721	5.24E-05	0.002757
mmu-miR-154-5p	-1.34006	6.792353	0.000115	0.005452
mmu-miR-337-3p	-1.7873	4.279888	0.000132	0.005709
mmu-miR-20a-5p	-1.41092	6.101225	0.000194	0.007664
mmu-miR-34a-5p	-1.02584	6.840127	0.00049	0.014504
mmu-miR-344b-3p	-1.16003	5.782174	0.000521	0.014537
mmu-miR-467d-3p	-1.27125	3.807484	0.002238	0.040798
mmu-miR-501-5p	-1.13212	3.756614	0.003367	0.049332
mmu-miR-296-5p	-1.01737	5.268559	0.003398	0.049332
Upregulated				
	logFC	logCPM	p-value	FDR
mmu-miR-148b-5p	1.584047	4.51305	3.49E-06	0.000915
mmu-miR-1981-5p	1.242745	6.153819	8.42E-06	0.001112
mmu-miR-744-5p	1.182076	9.015449	1.55E-05	0.001222
mmu-miR-488-3p	1.146546	9.126075	0.000427	0.014463
mmu-miR-873a-5p	1.043943	6.639535	0.00334	0.049332

logFC indicates log fold change and logCPM represents log counts per million indicative of expression levels; p-value and FDR < 0.05 were considered significant.

Supplementary Table 4: Differentially expressed miRNAs in wildtype (+/+) middle-aged (12-months) mice compared to wildtype young (3-months) mice.

Downregulated				
	logFC	logCPM	p-value	FDR
mmu-miR-296-5p	-1.80652	5.268559	2.42E-06	0.001145
mmu-miR-138-2-3p	-1.05163	4.550599	0.000126	0.019944
mmu-miR-669c-5p	-1.38239	3.69514	0.000341	0.032356
mmu-miR-1264-5p	-1.68777	6.203115	0.000797	0.047705
mmu-miR-204-5p	-1.52194	11.8411	0.000882	0.047705
mmu-let-7c-5p	-1.03125	14.47345	0.000906	0.047705
Upregulated				
	logFC	logCPM	p-value	FDR
mmu-miR-375-3p	2.935488	7.780796	1.07E-05	0.002526
mmu-miR-152-3p	1.097024	8.901353	0.000455	0.03592

logFC indicates log fold change and logCPM represents log counts per million indicative of expression levels; p-value and FDR < 0.05 were considered significant.

Supplementary Table 5: Pathway analysis of pathways associated with downregulated miRNAs in df/df middle-aged mice compared to df/df young mice.

KEGG pathway	p-value	#genes	#miRNAs
TGF-beta signaling pathway	8.74E-07	33	13
Prolactin signaling pathway	3.60E-06	29	13
Signaling pathways regulating pluripotency of stem cells	5.28E-06	43	12
Phosphatidylinositol signaling system	6.29E-06	31	11
Type II diabetes mellitus	8.52E-06	24	11
Neurotrophin signaling pathway	2.52E-05	45	13
Hippo signaling pathway	8.60E-05	48	14
MAPK signaling pathway	9.98E-05	74	14
Endocytosis	9.98E-05	66	14
ErbB signaling pathway	0.001699	27	13
FoxO signaling pathway	0.001699	43	13
cGMP-PKG signaling pathway	0.001718	51	13
Insulin signaling pathway	0.001718	44	13
Protein processing in endoplasmic reticulum	0.003255	47	12
AMPK signaling pathway	0.003255	39	12
Axon guidance	0.004837	41	13
PI3K-Akt signaling pathway	0.005777	82	13
Focal adhesion	0.006587	56	13
mTOR signaling pathway	0.006826	22	10
Long-term potentiation	0.006826	23	13
Dopaminergic synapse	0.006864	37	13
cAMP signaling pathway	0.007276	53	13
Rap1 signaling pathway	0.010348	54	12
Ras signaling pathway	0.01085	54	13
Ubiquitin mediated proteolysis	0.016322	42	14
GnRH signaling pathway	0.018167	26	13
Wnt signaling pathway	0.022807	38	14
TNF signaling pathway	0.026458	31	13
Regulation of actin cytoskeleton	0.038909	53	13

Supplementary Table 6: Pathway analysis of pathways associated with upregulated miRNAs in df/df middle-aged mice compared to df/df young mice.

KEGG pathway	p-value	#genes	#miRNAs
Fatty acid elongation	7.76E-05	3	2
Long-term depression	0.040991	7	3

#genes indicates total genes targeted by #miRNAs. Refer to Table 1 for list of downregulated miRNAs.

Supplementary Table 7: Pathway analysis of pathways associated with upregulated miRNAs in wildtype (+/+) middle-aged mice compared to wildtype young mice.

KEGG pathway	p-value	#genes	#miRNAs
Hippo signaling pathway	7.75E-07	16	2
PI3K-Akt signaling pathway	0.00056	27	2
Glycosaminoglycan biosynthesis - chondroitin sulfate / dermatan sulfate	0.003713	2	1
FoxO signaling pathway	0.003713	14	2
Thyroid hormone signaling pathway	0.013155	10	2
Glycosphingolipid biosynthesis - lacto and neolacto series	0.01711	1	1
Focal adhesion	0.021882	16	2
AMPK signaling pathway	0.035183	10	2
Regulation of actin cytoskeleton	0.035183	17	2
Insulin signaling pathway	0.035183	12	2
Signaling pathways regulating pluripotency of stem cells	0.039991	10	2

#genes indicates total genes targeted by #miRNAs. Refer to Table 1 for list of downregulated miRNAs.

Supplementary Table 8: Pathway analysis of pathways associated with downregulated miRNAs in wildtype (+/+) middle-aged mice compared to wildtype young mice.

KEGG pathway	p-value	#genes	#miRNAs
ECM-receptor interaction	9.21E-10	8	2
MAPK signaling pathway	0.004421	33	5
cGMP-PKG signaling pathway	0.006595	26	6
Lysine degradation	0.010529	7	3
Axon guidance	0.024395	21	6
Signaling pathways regulating pluripotency of stem cells	0.045223	18	4
Insulin signaling pathway	0.045223	19	4
mTOR signaling pathway	0.045223	11	5
PI3K-Akt signaling pathway	0.045223	35	5
Neurotrophin signaling pathway	0.045223	17	5

#genes indicates total genes targeted by #miRNAs. Refer to Table 1 for list of downregulated miRNAs.

Supplementary Table 9: Pathway analysis of pathways associated with upregulated miRNAs in df/df/APP/PS1 mice.

KEGG pathway	p-value	#genes	#miRNAs
Adherens junction	0.001011	10	3
Cell adhesion molecules (CAMs)	0.001011	11	4
Glycosphingolipid biosynthesis - lacto and neolacto series	0.001912	2	2
Long-term depression	0.001912	7	3
Primary immunodeficiency	0.005399	5	3
cGMP-PKG signaling pathway	0.005399	17	4
Regulation of actin cytoskeleton	0.005399	15	4
Endocytosis	0.006652	21	4
mTOR signaling pathway	0.014317	9	3
Glycosaminoglycan biosynthesis - heparan sulfate / heparin	0.018275	2	2
FoxO signaling pathway	0.030803	12	4

#genes indicates total genes targeted by #miRNAs. Refer to Table 2 for list of miRNAs.

Supplementary Table 10: miRNA expression patterns significantly altered in young df/+/APP/PS1 and df/df normalized to wildtype (+/+) mice as well as df/df/APP/PS1 mice normalized to df/df mice.

microRNA	Df/+/APP/PS1	Df/df	Df/df/APP/PS1
mmu-miR-144-5p		↓	↑
mmu-miR-488-3p		↑	
mmu-miR-296-5p		↑	
mmu-miR-7080-3p	↑	↑	
mmu-miR-6945-5p	↑		↓

p-value and FDR < 0.05 were considered significant.

Supplementary Table 11: Differentially expressed miRNAs in df/+/APP/PS1 middle-aged (12-months) mice compared to wildtype (+/+) middle-aged (12-months) mice.

Downregulated				
	logFC	logCPM	p-value	FDR
mmu-miR-375-3p	-3.38781	7.780796	7.72E-08	3.66E-05
mmu-miR-135a-5p	-1.05889	10.67297	5.69E-05	0.001928
mmu-miR-200c-3p	-4.52554	6.171858	9.35E-05	0.002954
mmu-miR-1957a	-1.30567	4.620322	0.000257	0.005792
mmu-miR-141-3p	-4.46763	4.961615	0.000459	0.007772
mmu-miR-200b-3p	-2.66643	7.87795	0.000929	0.012947
mmu-miR-183-5p	-2.54519	7.694231	0.007469	0.05246
Upregulated				
	logFC	logCPM	p-value	FDR
mmu-miR-1a-3p	2.905976	10.49826	2.47E-06	0.000553
mmu-miR-1b-5p	2.848746	6.677805	3.50E-06	0.000553
mmu-miR-29b-3p	1.249117	11.4522	4.73E-06	0.00056
mmu-let-7b-5p	1.368688	12.21319	1.21E-05	0.000858
mmu-miR-376a-3p	1.16266	7.844395	1.27E-05	0.000858
mmu-miR-206-3p	3.026847	3.992233	1.80E-05	0.001057
mmu-miR-219b-3p	1.880785	3.827941	2.01E-05	0.001057
mmu-miR-211-5p	1.742023	3.308976	2.41E-05	0.001142
mmu-miR-219a-5p	1.945132	3.778159	3.83E-05	0.001511
mmu-miR-204-3p	2.695174	3.535912	5.38E-05	0.001928
mmu-miR-669a-5p	1.73485	2.905534	0.000101	0.002977
mmu-miR-551b-3p	1.271694	4.902125	0.000136	0.003593
mmu-miR-187-3p	1.003512	6.510996	0.000296	0.006101
mmu-miR-331-3p	1.110888	7.122459	0.000338	0.006672
mmu-miR-669c-5p	1.307198	3.69514	0.000404	0.007365
mmu-miR-125a-5p	1.038551	13.30361	0.000389	0.007365
mmu-miR-142a-3p	1.311823	5.523477	0.000448	0.007772
mmu-miR-451a	2.053095	7.734843	0.000508	0.008311
mmu-let-7b-3p	1.247808	5.377523	0.001734	0.020048
mmu-miR-3065-5p	1.130459	4.789927	0.001921	0.021178
mmu-miR-298-5p	1.113258	6.40976	0.001902	0.021178
mmu-miR-669p-5p	1.228656	2.948003	0.004451	0.038137
mmu-miR-342-5p	1.028646	4.056786	0.004506	0.038137
mmu-miR-144-3p	1.809807	4.938562	0.005498	0.04343

logFC indicates log fold change and logCPM represents log counts per million indicative of expression levels; p-value and FDR < 0.05 were considered significant.

Supplementary Table 12: Differentially expressed miRNAs in df/df middle-aged (12-months) mice compared to wildtype (+/+) middle-aged (12-months) mice.

Downregulated				
	logFC	logCPM	p-value	FDR
mmu-miR-34a-5p	-2.5502	6.840127	1.15E-18	5.44E-16
mmu-miR-219a-2-3p	-2.07982	10.18031	1.12E-11	1.06E-09
mmu-miR-146a-5p	-1.78183	8.291832	1.36E-11	1.07E-09
mmu-miR-219b-5p	-2.00182	6.094238	9.65E-10	5.08E-08
mmu-miR-375-3p	-4.37157	7.780796	1.09E-09	5.16E-08
mmu-miR-22-5p	-1.67893	7.554657	2.33E-09	8.48E-08
mmu-miR-21a-5p	-1.23115	12.84453	4.09E-08	1.02E-06
mmu-miR-3065-3p	-2.03589	4.222469	2.35E-07	5.06E-06
mmu-miR-872-3p	-1.35014	6.416584	4.06E-07	8.27E-06
mmu-miR-598-3p	-1.05147	8.292758	6.25E-06	0.00011
mmu-miR-181a-1-3p	-1.14286	7.37391	9.14E-06	0.000144
mmu-miR-28a-5p	-1.08912	6.943083	1.15E-05	0.000176
mmu-miR-362-3p	-1.33516	6.3329	1.34E-05	0.000199
mmu-miR-135a-5p	-1.18776	10.67297	2.29E-05	0.00031
mmu-miR-219b-3p	-2.56775	3.827941	3.00E-05	0.000383
mmu-miR-99b-5p	-1.07723	11.4221	3.07E-05	0.000383
mmu-miR-338-5p	-1.03542	9.326232	4.79E-05	0.000516
mmu-miR-484	-1.08831	7.520804	6.62E-05	0.000654
mmu-miR-378a-3p	-1.31311	8.450034	8.03E-05	0.000761
mmu-miR-369-3p	-1.02191	12.37518	0.000114	0.000999
mmu-miR-344b-3p	-1.22773	5.782174	0.000166	0.001401
mmu-miR-190a-5p	-1.34202	6.397593	0.000196	0.001546
mmu-miR-301a-3p	-1.16343	6.137288	0.000307	0.002272
mmu-miR-299a-3p	-1.06511	4.67525	0.000312	0.002273
mmu-miR-381-3p	-1.06066	10.29398	0.00046	0.003157
mmu-miR-200c-3p	-4.30951	6.171858	0.000564	0.003765
mmu-miR-544-5p	-1.27172	4.862943	0.000641	0.004106
mmu-miR-154-5p	-1.10448	6.792353	0.001034	0.006124
mmu-miR-200b-3p	-2.68302	7.87795	0.002054	0.010876
mmu-miR-1191a	-1.23334	2.985399	0.002332	0.011979
mmu-miR-99b-3p	-1.15161	5.213117	0.00235	0.011979
mmu-miR-219a-5p	-1.87746	3.778159	0.002405	0.012126
mmu-miR-34c-5p	-1.53251	9.479192	0.002437	0.012161
mmu-miR-181b-2-3p	-1.07792	3.603542	0.002554	0.012482
mmu-miR-362-5p	-1.02055	5.669088	0.002538	0.012482
mmu-miR-19b-3p	-1.10898	7.259701	0.003568	0.016107
mmu-miR-19a-3p	-1.54335	3.213721	0.004369	0.018827
mmu-miR-20a-5p	-1.0343	6.101225	0.004705	0.019913
mmu-miR-5121	-1.14655	3.917791	0.006499	0.025673
mmu-miR-467d-3p	-1.11852	3.807484	0.006905	0.026827
mmu-miR-210-3p	-1.37242	3.838759	0.007879	0.029641
mmu-miR-10a-5p	-1.04365	4.604753	0.009644	0.034853
mmu-miR-141-3p	-3.15924	4.961615	0.014703	0.047736

Upregulated				
	logFC	logCPM	p-value	FDR
mmu-miR-496a-3p	1.658008	6.31463	2.46E-13	5.83E-11
mmu-miR-298-5p	2.616231	6.40976	1.48E-12	1.75E-10
mmu-miR-666-5p	1.814256	6.995841	1.20E-12	1.75E-10
mmu-miR-488-3p	2.051384	9.126075	6.07E-11	4.11E-09
mmu-miR-412-5p	1.416107	7.087957	5.02E-10	2.97E-08
mmu-miR-410-5p	2.651807	3.267332	1.29E-09	5.57E-08
mmu-miR-3078-5p	2.231532	3.732537	2.28E-09	8.48E-08
mmu-miR-296-5p	2.238627	5.268559	3.96E-09	1.34E-07
mmu-miR-770-5p	1.850373	4.624784	8.45E-09	2.55E-07
mmu-miR-376b-3p	1.533847	11.34841	8.60E-09	2.55E-07
mmu-miR-3071-3p	1.696844	8.141422	9.86E-09	2.75E-07
mmu-miR-3059-5p	1.447154	6.864501	1.65E-08	4.34E-07
mmu-miR-770-3p	1.586937	7.421687	7.90E-08	1.87E-06
mmu-miR-323-5p	1.913853	4.488324	1.09E-07	2.47E-06
mmu-miR-744-5p	1.311358	9.015449	4.19E-07	8.27E-06
mmu-miR-1981-5p	1.256016	6.153819	2.26E-06	4.11E-05
mmu-miR-410-3p	1.243678	11.27004	8.41E-06	0.000137
mmu-miR-504-5p	1.625322	4.856346	2.23E-05	0.00031
mmu-miR-130a-3p	1.127099	6.979033	2.84E-05	0.000374
mmu-miR-139-3p	1.435822	4.932857	3.23E-05	0.000392
mmu-miR-873a-3p	1.244555	4.810445	4.13E-05	0.000478
mmu-miR-690	1.415605	5.305764	4.68E-05	0.000516
mmu-miR-873a-5p	1.375077	6.639535	5.26E-05	0.000554
mmu-miR-31-5p	1.365083	7.618326	5.95E-05	0.000613
mmu-miR-3072-3p	1.077016	5.201834	7.81E-05	0.000755
mmu-miR-7b-3p	1.690247	3.544128	0.000106	0.000969
mmu-miR-136-5p	1.928314	9.036907	0.00016	0.001376
mmu-miR-29b-3p	1.058792	11.4522	0.000171	0.001418
mmu-miR-488-5p	1.68101	3.477176	0.000193	0.001546
mmu-miR-351-5p	1.027438	6.147513	0.000238	0.001846
mmu-miR-7a-5p	1.051844	13.75342	0.000327	0.002334
mmu-miR-377-3p	1.697556	5.92247	0.000472	0.003193
mmu-miR-433-3p	1.034738	9.584574	0.000585	0.003853
mmu-miR-7080-3p	1.457616	3.476762	0.000975	0.005847
mmu-miR-760-3p	1.475357	3.428758	0.001421	0.008017
mmu-miR-137-5p	1.121372	4.127183	0.001828	0.009848
mmu-miR-1251-5p	1.428141	3.029926	0.00336	0.015463
mmu-miR-700-5p	1.163195	3.656029	0.003723	0.016648
mmu-miR-342-5p	1.097946	4.056786	0.003758	0.016648
mmu-miR-3084-5p	1.077778	3.143999	0.004496	0.019201
mmu-miR-300-5p	1.013899	4.182547	0.008837	0.032724
mmu-miR-344c-3p	1.012361	5.120167	0.009706	0.034853
mmu-miR-3085-3p	1.182477	3.047014	0.015232	0.048783

logFC indicates log fold change and logCPM represents log counts per million indicative of expression levels; p-value and FDR < 0.05 were considered significant.

Supplementary Table 13: Differentially expressed miRNAs in df/df/APP/PS1 middle-aged (12-months) mice compared to df/+/APP/PS1 middle-aged (12-months) mice.

Downregulated				
	logFC	logCPM	PValue	FDR
mmu-miR-374b-5p	-2.41496	7.943131	2.23E-12	7.75E-10
mmu-miR-1b-5p	-3.58833	6.677805	1.72E-08	2.04E-06
mmu-miR-1a-3p	-3.45363	10.49826	4.62E-08	4.38E-06
mmu-miR-34a-5p	-1.3858	6.840127	6.35E-08	5.02E-06
mmu-miR-219b-3p	-2.43169	3.827941	1.23E-07	8.32E-06
mmu-miR-467a-5p	-1.67519	5.817518	8.02E-07	3.12E-05
mmu-miR-1983	-1.09403	7.804075	8.56E-07	3.12E-05
mmu-miR-22-3p	-1.49195	12.19987	1.19E-06	3.76E-05
mmu-miR-219a-5p	-2.29728	3.778159	1.63E-06	4.79E-05
mmu-miR-669c-5p	-1.91214	3.69514	3.39E-06	8.45E-05
mmu-miR-299a-5p	-1.09133	5.254931	5.39E-06	0.000116
mmu-miR-29b-3p	-1.22381	11.4522	7.27E-06	0.000144
mmu-miR-142a-3p	-1.61275	5.523477	2.40E-05	0.000393
mmu-miR-206-3p	-2.95884	3.992233	2.59E-05	0.000409
mmu-miR-540-5p	-1.51357	3.481218	4.38E-05	0.000629
mmu-miR-129-1-3p	-1.05937	8.26967	5.14E-05	0.000696
mmu-miR-98-3p	-1.61498	4.227327	7.15E-05	0.000941
mmu-miR-338-3p	-1.19013	10.31861	0.000163	0.001713
mmu-miR-15a-5p	-1.04424	8.643509	0.000178	0.001792
mmu-miR-186-3p	-1.86082	3.000975	0.000204	0.001932
mmu-miR-32-5p	-1.66448	5.715804	0.000241	0.00224
mmu-miR-381-3p	-1.03304	10.29398	0.000293	0.002522
mmu-miR-3065-5p	-1.29078	4.789927	0.000482	0.004012
mmu-miR-669p-5p	-1.55699	2.948003	0.000494	0.004041
mmu-miR-144-3p	-2.28267	4.938562	0.000653	0.005076
mmu-miR-223-3p	-1.00372	5.303337	0.001025	0.007833
mmu-let-7b-3p	-1.32371	5.377523	0.001074	0.007838
mmu-miR-7689-3p	-1.03716	4.485849	0.002115	0.013735
mmu-let-7f-1-3p	-1.23385	3.704233	0.002591	0.015951
mmu-miR-153-3p	-1.05743	10.69411	0.004089	0.022027
mmu-miR-448-5p	-1.0744	4.366031	0.006873	0.030446
mmu-miR-451a	-1.54213	7.734843	0.007962	0.033702
mmu-miR-34b-5p	-1.60121	4.872446	0.008341	0.034986
mmu-miR-669a-5p	-1.03802	2.905534	0.011799	0.044742

Upregulated				
	logFC	logCPM	PValue	FDR
mmu-miR-412-5p	1.566057	7.087957	3.27E-12	7.75E-10
mmu-miR-488-3p	2.112891	9.126075	5.36E-12	8.46E-10
mmu-miR-488-5p	2.393364	3.477176	1.67E-07	9.90E-06
mmu-miR-666-5p	1.270472	6.995841	2.18E-07	1.15E-05
mmu-miR-344-3p	1.229254	8.740479	5.54E-07	2.40E-05
mmu-miR-30a-3p	1.258658	9.907382	1.18E-06	3.76E-05
mmu-miR-380-5p	1.279916	7.253146	1.72E-06	4.79E-05
mmu-miR-431-5p	1.125915	7.566675	7.94E-06	0.000151
mmu-miR-1957a	1.540065	4.620322	1.63E-05	0.000286
mmu-miR-135a-2-3p	1.594776	3.313596	2.09E-05	0.000354
mmu-miR-298-5p	1.390656	6.40976	3.91E-05	0.000598
mmu-miR-148b-3p	1.119173	9.985809	4.23E-05	0.000627
mmu-miR-450a-5p	1.048203	5.664682	8.31E-05	0.00101
mmu-miR-7b-5p	1.064321	12.16573	9.58E-05	0.001115
mmu-miR-30f	1.01548	4.382483	9.64E-05	0.001115
mmu-miR-148a-3p	1.024252	11.01273	0.000138	0.001484
mmu-miR-30e-3p	1.016299	10.00549	0.000172	0.001769
mmu-miR-3078-5p	1.173141	3.732537	0.002334	0.014557
mmu-miR-6236	1.08112	8.88245	0.002962	0.017549
mmu-miR-222-5p	1.086662	3.170687	0.003426	0.018881
mmu-miR-542-3p	1.44172	8.902629	0.006614	0.029803
mmu-miR-382-3p	1.213551	3.114667	0.006665	0.029803
mmu-miR-200b-3p	2.108197	7.87795	0.007504	0.032334
mmu-miR-182-5p	2.527841	9.036227	0.009195	0.037574
mmu-miR-6937-5p	1.044239	9.408945	0.012943	0.04793

logFC indicates log fold change and logCPM represents log counts per million indicative of expression levels; p-value and FDR < 0.05 were considered significant.

LIST OF REFERENCES

1. Campisi, J., *Aging, Cellular Senescence, and Cancer* Annual Review of Physiology 2012. **75**: p. 685-705.
2. *National Cancer Institute Dictionary of Cancer terms*. [cited 2021 May]; Available from: https://www.cancer.gov/publications/dictionaries/cancer-terms/def/hyperplasia.
3. López-Otín, C., Blasco, M.A., Partridge, L., Serrano, M., Kroemer, G., *The hallmarks of aging.* Cell 2013. **153**(6): p. 1194-1217.
4. Moskalev, A.A., Shaposhnikov, M.V., Plyusnina, E.N., Zhavoronkov, A., Budovsky, A., Yanai, H., Fraifeld, V.E., *The role of DNA damage and repair in aging through the prism of Koch-like criteria.* Ageing Research Reviews, 2013. **12**(2): p. 661-684.
5. Blackburn, E., Greider, C., Szostak, J., *Telomeres and telomerase: the path from maize, Tetrahymena and yeast to human cancer and aging.* Nature Medicine, 2006. **12**: p. 1133–1138.
6. Moore, L.D., Le, T., Fan, G. , *DNA Methylation and Its Basic Function.* Neuropsychopharmacology, 2013. **38**: p. 23-38.
7. Bannister, A., Kouzarides, T., *Regulation of chromatin by histone modifications.* Cell Research, 2011. **21**: p. 381-395.
8. Efeyan, A., Comb, W., Sabatini, D., *Nutrient-sensing mechanisms and pathways.* Nature, 2015. **517**: p. 302-310.
9. Bartke, A., *Impact of reduced insulin-like growth factor-1/insulin signaling on aging in mammals: novel findings.* Aging Cell 2008. **7**(3): p. 285-290.

10. Lamming, D., *Diminished mTOR signaling: a common mode of action for endocrine longevity factors.* Springer Plus 2014. **3**(735).

11. Khee S, Y.Y., Makpol S, *Expression of senescence-associated microRNAs and target genes in cellular aging and modulation by tocotrienol-rich fraction.* Oxidative Medicine and Cellular Longevity 2014.

12. Campisi, J., d'Adda di Fagagna, F., *Cellular senescence: when bad things happen to good cells* Nature Reviews. Molecular Cell Biology, 2007. **8**(9): p. 729-740.

13. Maréchal, A., Zou L., *DNA Damage Sensing by the ATM and ATR Kinases.* Cold Spring Harbor Perspectives in Biology, 2013. **5**(9).

14. Stein, G.H., Drullinger, L.F., Soulard, A., Dulić, V., *Differential roles for cyclin-dependent kinase inhibitors p21 and p16 in the mechanisms of senescence and differentiation in human fibroblasts.* Molecular and Cellular Biology, 1999. **19**(3): p. 2109-2117.

15. Engeland, K., *Cell cycle regulation: p53-p21-RB signaling.* Cell Death & Differentiation, 2022. **29**: p. 946-960.

16. Coppe JP, D.P., Krtolica A, Campisi J *The senescence-associated secretory phenotype: the dark side of tumor suppression.* Annual Review of Physiology, 2010 **5**: p. 99-118.

17. Saccon, T.D., Nagpal, R., Yadav, H., Cavalcante, M.B., Nunes, A.D.C., Schneider, A., Gesing, A., Hughes, B., Yousefzadeh, M., Tchkonia, T., Kirkland, J.L., Niedernhofer, L.J., Robbins, P.D., Masternak, M.M., *Senolytic Combination of Dasatinib and Quercetin Alleviates Intestinal Senescence and Inflammation and Modulates the Gut Microbiome in Aged Mice.* The Journals of Gerontology Series A: Biological Sciences and Medical Sciences, 2021. **76**(11): p. 1895-1905.

18. Di Micco, R., Krizhanovsky, V., Baker, D., d'Adda di Fagagna, F. , *Cellular senescence in ageing: from mechanisms to therapeutic opportunities.* Nature Reviews Molecular Cell Biology volume, 20221. **22**: p. 75-95.

19. Darcy, J., McFadden, S., Bartke, A., *Altered structure and function of adipose tissue in long-lived mice with growth hormone-related mutations.* Adipocyte 2017. **6**(2): p. 69-75.

20. Dusatkova, P., Pfäffle, R., Brown, M., kulevich, N., Arnhold, I.J., Kalina, M.A., Kot, K., Krzisnik, C., Lemos, M.C., Malikova, J., Navardauskaite, R., Obermannova, B., Pribilincova, Z., Sallai, A., Stipancic, G., Verkauskiene, R., Cinek, O., Blum, W.F., Parks, J.S., Austerlitz, F., Lebl, J. , *Genesis of two most prevalent PROP1 gene variants causing combined pituitary hormone deficiency in 21 populations.* European Journal of Human Genetics, 2016. **24**(3): p. 415-420.

21. Bartke, A., Wright, J. C., Mattison, J. A., Ingram, D. K., Miller, R. A., Roth, G. S., *Extending the lifespan of long-lived mice.* Nature, 2001. **414**: p. 412.

22. Wiesenborn DS, A.J., King E, Masternak MM, *Insulin sensitivity in long-living Ames dwarf mice.* Age, 2014. **36**(5): p. 9709.

23. Masternak, M.M., Panici, J. A., Bonkowski, M. S., Hughes, L. F.,Bartke, A., *Insulin Sensitivity as a Key Mediator of Growth Hormone Actions on Longevity.* The Journals of Gerontology Series A: Biological Sciences and Medical Sciences, 2009. **64A**(5): p. 516-521.

24. Bartke, A., Brown-Borg, H. M., *Life Extension in the Dwarf Mouse.* Current Topics in Developmental Biology, 2004. **63**: p. 189-225.

25. Li, X., McPherson, M., Hager, M., Fang, Y., Bartke, A., Miller, R.A. , *Transient early life growth hormone exposure permanently alters brain, muscle, liver, macrophage, and adipocyte status in long-lived Ames dwarf mice.* FASEB 2022. **36**(7).

26. Brinkman, J.E., Tariq, M. A., Leavitt, L., Sharma, S. , *Physiology, Growth Hormone.* StatPearls 2022.

27. Menon, V., Zhi, X., Hossain, T., Bartke, A., Spong, A., Gesing, A., Masternak, M. M. , *The contribution of visceral fat to improved insulin signaling in Ames dwarf mice.* Aging cell 2014. **13**(3): p. 497-506.

28. He, L., Hannon, G., *MicroRNAs: small RNAs with a big role in gene regulation.* Nature Reviews. Genetics, 2004. **5**: p. 522-531.

29. MacFarlane, L.A., Murphy, P.A. , *MicroRNA: Biogenesis, Function, and Role in Cancer* Current Genomics 2010. **11**(7): p. 537-561.

30. Victoria, B., Dhahbi, J. M., Nunez Lopez, Y. O., Spinel, L., Atamna, H., Spindler, S. R., Masternak, M. M. , *Circulating microRNA signature of genotype-by-age interactions in the long-lived Ames dwarf mouse.* Aging cell 2015. **14**(6): p. 1055-1066.

31. Chen Y, W.X., *miRDB: an online database for prediction of functional microRNA targets.* Nucleic Acids Research, 2020(D1): p. D127-D131.

32. Avelar, R.A., Ortega, J. G., Tacutu, R., Tyler, E. J., Bennett, D., Binetti, P., Budovsky, A., Chatsirisupachai, K., Johnson, E., Murray, A., Shields, S., Tejada-Martinez, D., Thornton, D., Fraifeld, V. E., Bishop, C. L., de Magalhaes, J. P, *A multidimensional systems biology analysis of cellular senescence in aging and disease.* Genome Biology 2020. **21**(1): p. 91.

33. Tan, Y.X., Hong, Y., Jiang, S., Lu, M. N., Li, S., Chen, B., Zhang, L., Hu, T., Mao, R., Mei, R., & Xiyang, Y. B. , *MicroRNA-449a regulates the progression of brain aging by targeting SCN2B in SAMP8 mice.* International Journal of Molecular Medicine, 2020. **45**(4): p. 1091-1102.

34. Martinez, C.S., Piazza, V. G., González, L., Fang, Y., Bartke, A., Turyn, D., Miquet, J. G., Sotelo, A. I. , *Mitogenic signaling pathways in the liver of growth hormone (GH)-overexpressing mice during the growth period.* . Cell Cycle, 2016. **15**(5): p. 748-759.

35. *The top 10 Causes of Death*. 2020 [cited 2021 May]; Available from: https://www.who.int/news-room/fact-sheets/detail/the-top-10-causes-of-death.

36. Association, A.s., *2022 Alzheimer's Disease Facts and Figures*. 2022: Alzheimers Dement.

37. Nyul-Toth, A., DelFavero, J., Mukli, P., Tarantini, A., Ungvari, A., Yabluchanskiy, A., Csiszar, A., Ungvari, Z., & Tarantini, S., *Early manifestation of gait alterations in the Tg2576 mouse model of Alzheimer's disease.* GeroScience, 2021. **43**(4): p. 1947-1957.

38. Weller, J., Budson, A. , *Current understanding of Alzheimer's disease diagnosis and treatment.* F1000 Research, 2018. **7**.

39. Chen, G., Xu, Th., Yan, Y., Zhou, Y., Jiang, Y., Melcher, K., Xu, H. E. , *Amyloid beta: structure, biology and structure-based therapeutic development.* Acta Pharmacologica Sinica, 2017. **38**: p. 1205–1235.

40. Gong, C.X., Iqbal, K., *Hyperphosphorylation of microtubule-associated protein tau: a promising therapeutic target for Alzheimer disease.* Current Medicinal Chemistry, 2008. **15**(23): p. 2321-2328.

41. Darcy, J., Tseng, Y.H. , *ComBATing aging—does increased brown adipose tissue activity confer longevity?* GeroScience, 2019. **41**: p. 285-296.

42. Kang, C., *Senolytics and Senostatics: A Two-Pronged Approach to Target Cellular Senescence for Delaying Aging and Age-Related Diseases.* . Molecules and Cells 2019. **42**(12): p. 821-827.

43. Victoria B, L.Y., Masternak M *MicroRNAs and the Metabolic Hallmarks of Aging.* Molecular and Cellular Endocrinology 2017. **455**: p. 131-147.

44. Nunes, A.D.C., Weigl, M., Schneider, A., Noureddine, S., Yu, L., Lahde, C., Saccon, T. D., Mitra, K., Beltran, E., Grillari, J., Kirkland, J. L., Tchkonia, T., Robbins, P. D., Masternak, M. M. , *miR-146a-5p modulates cellular senescence and apoptosis in visceral adipose tissue of long-lived Ames dwarf mice and in cultured pre-adipocytes.* GeroScience, 2022. **44**(1): p. 503-518.

45. Stout, M.B., Tchkonia, T., Pirtskhalava, T., Palmer, A. K., List, E. O., Berryman, D. E., Lubbers, E. R., Escande, C., Spong, A., Masternak, M. M., Oberg, A. L., LeBrasseur, N. K., Miller, R. A., Kopchick, J. J., Bartke, A., & Kirkland, J. L. , *Growth hormone action predicts age-related white adipose tissue dysfunction and senescent cell burden in mice.* Aging, 2014. **6**(7): p. 575-586.

46. Naderi, N., Combellack, E. J., Griffin, M., Sedaghati, T., Javed, M., Findlay, M. W., Wallace, C. G., Mosahebi, A., Butler, P. E., Seifalian, A. M., & Whitaker, I. S., *The regenerative role of adipose-derived stem cells (ADSC) in plastic and reconstructive surgery.* International Wound Journal 2017. **14**(1): p. 112-124.

47. Nee K., N.Q., Kessenbrock K., *Signle Nuclei RNA Sequencing of Breast Adipose Tissue* Protocols.io, 2018.

48. Gimble J.M., G.F., *Adipose-derived adult stem cells: isolation, characterization, and differentiation potential.* Cytotherapy, 2003. **5**(5): p. 362-369.

49. Zheng, G., Terry, JM, Belgrader, P, Ryvkin, P, Bent, ZW, Wilson, R, Ziraldo, SB, Wheeler, TD, McDermott, GP, Zhu, J, Gregory, MT, Shuga, J, Montesclaros, L, Underwood, JG, Masquelier, DA, Nishimura, SY, Schnall-Levin, M, Wyatt, PW, Hindson, CM, Bharadwaj, R, Wong, A, Ness, KD, Beppu, LW, Deeg, HJ, McFarland, C, Loeb, KR, Valente, WJ, Ericson, NG, Stevens, EA, Radich, JP, Mikkelsen, TS, Hindson, BJ, Bielas, JH, *Massively parallel digital transcriptional profiling of single cells.* Nature Communications, 2017. **8**.

50. Sárvári A.K., V.H.E.L., Markussen L.K., Gammelmark E., Marcher A.B., Ebbesen M.F., Nielsen R., Brewer J.R., Madsen J.G.S., Mandrup S. , *Plasticity of Epididymal Adipose Tissue in Response to Diet-Induced Obesity at Single-Nucleus Resolution.* Cell Metabolism, 2021. **33**(2): p. 437-453.

51. Satija, R., Farrell, JA, Gennert, D, Schier, AF, Regev, A, *Spatial reconstruction of single-cell gene expression data.* Nature Biotechnology, 2015. **33**(5): p. 495-502.

52. Korsunsky, I., Millard, N, Fan, J, Slowikowski, K, Zhang, F, Wei, K, Baglaenko, Y, Brenner, M, Loh, PR, Raychaudhuri, S, *Fast, sensitive and accurate integration of single-cell data with Harmony.* Nature Methods, 2019. **16**(12): p. 1289-1296.

53. Stuart, T., Butler, A, Hoffman, P, Hafemeister, C, Papalexi, E, Mauck, WM 3rd, Hao, Y, Stoeckius, M, Smibert, P, Satija, R., *Comprehensive Integration of Single-Cell Data.* Cell, 2019. **177**(7): p. 1888-1902.

54. McDavid, A., Finak, G, Chattopadyay, PK, Dominguez, M, Lamoreaux, L, Ma, SS, Roederer, M, Gottardo, R, *Data exploration, quality control and testing in single-cell qPCR-based gene expression experiments.* Bioinformatics, 2013. **15**(29).

55. Ritchie, M., Phipson, B, Wu, D, Hu, Y, Law, CW, Shi, W, Smyth, GK, *limma powers differential expression analyses for RNA-sequencing and microarray studies.* Nucleic Acids Research, 2015. **43**(7).

56. Yu, G., Wang, LG, Han, Y, He, QY, *clusterProfiler: an R package for comparing biological themes among gene clusters.* OMICS, 2012. **16**(5): p. 284-287.

57. Slenter, D., Kutmon, M, Hanspers, K, Riutta, A, Windsor, J, Nunes, N, Mélius, J, Cirillo, E, Coort, SL, Digles, D, Ehrhart, F, Giesbertz, P, Kalafati, M, Martens, M, Miller, R, Nishida, K, Rieswijk, L, Waagmeester, A, Eijssen, LMT, Evelo, CT, Pico, AR, Willighagen, EL, *WikiPathways: a multifaceted pathway database bridging metabolomics to other omics research.* Nucleic Acids Research, 2018. **46**(D1): p. D661-D667.

58. Moon, K., van Dijk, D, Wang, Z, Gigante, S, Burkhardt, DB, Chen, WS, Yim, K, Elzen, AVD, Hirn, MJ, Coifman, RR, Ivanova, NB, Wolf, G, Krishnaswamy, S, *Visualizing structure and transitions in high-dimensional biological data.* Nature Biotechnology, 2019. **37**(12): p. 1482-1492.

59. Albergante, L., Mirkes, E, Bac, J, Chen, H, Martin, A, Faure, L, Barillot, E, Pinello, L, Gorban, A, Zinovyev, A *Robust and Scalable Learning of Complex Intrinsic Dataset Geometry via ElPiGraph.* Entropy (Basel), 2020. **22**(3).

60. Hepler C., S.B., Zhang Q., Henry G.H., Shao M., Vishvanath L., Ghaben A.L., Mobley A.B., Strand D., Hon G.C., Gupta R.K., *Identification of functionally distinct fibro-*

inflammatory and adipogenic stromal subpopulations in visceral adipose tissue of adult mice. eLife, 2018. **7**.

61. Kanehisa, M., Sato, Y., Kawashima, M., Furumichi, M., Tnabe, M., *KEGG as a reference resource for gene and protein annotation.* Nucleic Acids Research, 2016. **44**: p. D457-D462.

62. Barnes PJ, B.J., Donnelly LE, *Senescence as a Mechanism and Target in Chronic Lung Diseases.* American Journal of Respiratory and Critical Care Medicine 2019. **200**(5): p. 556-564.

63. Martins R., L.G.J., Link W., *Long live FOXO: unraveling the role of FOXO proteins in aging and longevity.* Aging cell 2016. **15**(2): p. 196-207.

64. Merrick D., S.A., Irgebay Z., Okada C., Calvert C., Morley M.P., Percec I., Seale P., *Identification of a mesenchymal progenitor cell hierarchy in adipose tissue.* Science, 2019. **364**(6438).

65. Burl, R.B., Ramseyer, V. D., Rondini, E. A., Pique-Regi, R., Lee, Y. H., Granneman, J. G. , *Deconstructing Adipogenesis Induced by β3-Adrenergic Receptor Activation with Single-Cell Expression Profiling.* Cell Metabolism 2018. **28**(2): p. 300-309.

66. Schwalie P.C., D.H., Zachara M., Russeil J., Alpern D., Akchiche N., Caprara C., Sun W., Schlaudraff K.U., Soldati G., Wolfrum C., Deplancke B., *A stromal cell population that inhibits adipogenesis in mammalian fat depots.* . Nature 2018. **559**(7712): p. 103-108.

67. Hill, C.M., Fang, Y., Miquet, J. G., Sun, L. Y., Masternak, M. M., Bartke, A. , *Long-lived hypopituitary Ames dwarf mice are resistant to the detrimental effects of high-fat diet on metabolic function and energy expenditure.* Aging cell 2016. **15**(3): p. 509-521.

68. Park J.H., L.N.K., Lim H.J., Ji S.T., Kim Y.J., Bi Jang W., Kim D.Y., Kang S., Yun J., Ha J.S., Kim H., Lee D., Baek S.H., Kwon S.M. , *Pharmacological inhibition of mTOR attenuates replicative cell senescence and improves cellular function via regulating the STAT3-PIM1 axis in human cardiac progenitor cells.* Experimental and Molecular Medicine 2020. **52**: p. 615-628.

69. Harrison D.E., S.R., Sharp Z.D., Nelson J.F., Astle C.M., Flurkey K., Nadon N.L., Wilkinson J.E., Frenkel K., Carter C.S., Pahor M., Javors M.A., Fernandez E., Miller R.A., *Rapamycin fed late in life extends lifespan in genetically heterogeneous mice.* Nature, 2009. **460**: p. 392-395.

70. Gesing A, A.-R.K., Bartke A, Masternak MM, *Growth hormone abolishes beneficial effects of calorie restriction in long-lived Ames dwarf mice.* Experimental Gerontology, 2014. **58**: p. 219-229.

71. El-Badawy A., A.M., Abdelbaset R., Sherif S.N., Abo-Elela M., Ghallab Y.H., Abdelhamid H., Ismail Y., El-Badri N. , *Adipose Stem Cells Display Higher Regenerative Capacities and More Adaptable Electro-Kinetic Properties Compared to Bone Marrow-Derived Mesenchymal Stromal Cells.* Scientific Reports 2016. **6**.

72. Paik S., J.H.S., Lee S., Yoon D.S., Park M.S., Lee J.W. , *miR-449a regulates the chondrogenesis of human mesenchymal stem cells through direct targeting of lymphoid enhancer-binding factor-1.* Stem Cells and Development 2012. **21**(18): p. 3298-3308.

73. Noonan, E.J., Place, R. F., Basak, S., Pookot, D., Li, L. C. , *miR-449a causes Rb-dependent cell cycle arrest and senescence in prostate cancer cells.* Oncotarget, 2010. **1**(5): p. 349-358.

74. Tan, J., Xu, Y., Han, F., Ye, X., *Genetical modification on adipose-derived stem cells facilitates facial nerve regeneration.* Aging, 2019. **11**(3): p. 908-920.

75. Kunze, K.N., Burnett, R. A., Wright-Chisem, J., Frank, R. M., Chahla, J. , *Adipose-Derived Mesenchymal Stem Cell Treatments and Available Formulations.* Current Reviews in Musculoskeletal Medicine 2020. **13**(3): p. 264-280.

76. Ma T., S.J., Zhao Z., Lei W., Chen Y., Wang X., Yang J., Shen Z., *A brief review: adipose-derived stem cells and their therapeutic potential in cardiovascular diseases.* Stem Cell Research & Therapy, 2017. **8**(1): p. 124.

77. Organization, W.H. *The top 10 causes of death* 2020; Available from: https://www.who.int/news-room/fact-sheets/detail/the-top-10-causes-of-death.

78. Kendra L. Puig, J.A.K., Whitney Franklin, Sharlene G. Rakoczy, Giulio Taglialatela, Holly M. Brown-Borg, and Colin K. Combs *The Ames Dwarf Mutation Attenuates Alzheimer's Disease Phenotype of APP/PS1 mice.* Neurobiology of Aging, 2016. **40**: p. 22-40.

79. Schrag, M., et al., *Hippocampus of Ames dwarf mice is resistant to beta-amyloid-induced tau hyperphosphorylation and changes in apoptosis-regulatory protein levels.* Hippocampus, 2008. **18**(3): p. 239-44.

80. Pushpakumar, S., et al., *Exogenous hydrogen sulfide and miR-21 antagonism attenuates macrophage-mediated inflammation in ischemia reperfusion injury of the aged kidney.* Geroscience, 2021. **43**(3): p. 1349-1367.

81. Liu, C.G., Wang, J. L., Li, L., Xue, L. X., Zhang, Y. Q., Wang, P. C. , *MicroRNA-135a and -200b, potential Biomarkers for Alzheimer's disease, regulate β secretase and amyloid precursor protein.* Brain Research, 2014. **1583**: p. 55-64.

82. Rueda A, B.G., Lebrón R, Gómez-Martín C, Alganza Á, Oliver JL, Hackenberg M. , *sRNAtoolbox: an integrated collection of small RNA research tools.* Nucleic Acids Research, 2015. **43**(W1): p. W467-473.

83. Robinson, M.D., McCarthy, D.J., Smyth, G.K., *edgeR: a Bioconductor package for differential expression analysis of digital gene expression data.* . Bioinformatics, 2010. **26**(1): p. 139-140.

84. Vlachos, I.S., Zagganas, K., Paraskevopoulou, M. D., Georgakilas, G., Karagkouni, D., Vergoulis, T., Dalamagas, T., & Hatzigeorgiou, A. G. (2015). DIANA-miRPath v3.0: deciphering microRNA function with experimental support. Nucleic acids research, 43(W1), W460–W466. https://doi.org/10.1093/nar/gkv403, *DIANA-miRPath v3.0: deciphering microRNA function with experimental support.* Nucleic Acids Research, 2015. **43**.

85. Liu, W., and Wang, X., *Prediction of functional microRNA targets by integrative modeling of microRNA binding and target expression data.* Genome Biology 2019. **20**(1).

86. Ando, K., Houben, S., Homa, M., de Fisenne, M.A., Potier, M.C., Erneux, C., Brion, J.P., Leroy, K., *Alzheimer's Disease: Tau Pathology and Dysfunction of Endocytosis.* Frontiers in Molecular Neuroscience, 2020. **13**.

87. Tian, N., Cao, Z., Zhang, Y. , *MiR-206 decreases brain-derived neurotrophic factor levels in a transgenic mouse model of Alzheimer's disease.* Neuroscience Bulletin 2014. **30**(2): p. 191-197.

88. Zeng, L., Jiang, H. L., Ashraf, G. M., Li, Z. R., Liu, R. , *MicroRNA and mRNA profiling of cerebral cortex in a transgenic mouse model of Alzheimer's disease by RNA sequencing.* Neural Regeneration Research, 2021.

89. Zhang, Q.S., Liu, W., Lu, G. X. , *miR-200a-3p promotes b-Amyloid-induced neuronal apoptosis through down-regulation of SIRT1 in Alzheimer's disease.* Journal of Biosciences 2017. **42**(3): p. 397-404.

90. Du, S., Zheng, H. , *Role of FoxO transcription factors in aging and age-related metabolic and neurodegenerative diseases.* Cell & Bioscience, 2021. **11**.

91. Woodling, N.S., Rajasingam, A., Minkley, L. J., Rizzo, A., Partridge, L. , *Independent glial subtypes delay development and extend healthy lifespan upon reduced insulin-PI3K signalling.* BMC Biology, 2020. **18**.

92. Paradis, E., Douillard, H., Koutroumanis, M., Goodyer, C., LeBlanc, A., *Amyloid β Peptide of Alzheimer's Disease Downregulates Bcl-2 and Upregulates Bax Expression in Human Neurons.* The Journal of Neuroscience 1996. **16**(23): p. 7533-7539.

93. Callens, M., Kraskovskaya, N., Derevtsova, K., Annaert, W., Bultynck, G., Bezprozvanny, I., Vervliet, T., *The role of Bcl-2 proteins in modulating neuronal Ca2+ signaling in health and in Alzheimer's disease.* Biochimica et Biophysica Acta (BBA) - Molecular Cell Research, 2021. **1868**(6).

94. Sierksma, A., Lu, A., Salta, E., Eynden, E. V., Callaerts-Vegh, Z., D'Hooge, R., Blum, D., Buee, L., Fiers, M., Strooper, B.D. , *Deregulation of neuronal miRNAs induced by amyloid-β or TAU pathology.* Molecular Neurodegeneration 2018. **13**(54).

95. Cha, D.J., Mengel, D., Mustapic, M., Liu, W., Selkoe, D. J., Kapogiannis, D., Galasko, D., Rissman, R. A., Bennet, D. A., Walsh, D. M., *miR-212 and miR-132 Are Downregulated in Neurally Derived Plasma Exosomes of Alzheimer's Patients.* Frontiers in Neuroscience 2019.

96. Lee, J., Lau, KF, Perkinton, MS, Standen, CL, Shemilt, SJ, Mercken, L, Cooper, JD, McLoughlin, DM, Miller, CC., *The neuronal adaptor protein X11alpha reduces Abeta levels in the brains of Alzheimer's APPswe Tg2576 transgenic mice.* Journal of Biological Chemistry 2003. **278**(47).

97. Yuan, X.Z., Sun, S., Tan, C.C., Yu, J.T., Tan, L. , *The Role of ADAM10 in Alzheimer's Disease.* Journal of Alzheimer's Disease, 2017. **58**(2).

98. Delay, C., Mandemakers, W., Hebert, S. S. , *MicroRNAs in Alzheimer's disease.* Neurobiology of Disease, 2012. **46**(2): p. 285-290.

99. Wei, W., Whang, Z.W., Ma, L.N., Zhang, T.T., Cao, Y., Li, H. , *MicroRNAs in Alzheimer's Disease: Function and Potential Applications as Diagnostic Biomarkers.* Frontiers in Molecular Neuroscience 2020.